Revista Mexicana de Astronomía y Astrofísica, Volumen 2, Agosto 1977

PHOTOELECTRIC PHOTOMETRY AND PHYSICAL CONDITIONS OF PLANETARY NEBULAE

SILVIA TORRES-PEIMBERT*
AND
MANUEL PEIMBERT*

Instituto de Astronomía
Universidad Nacional Autónoma de México
Received 1976 December 16

RESUMEN

Se presentan observaciones de espectrofotometría fotoeléctrica de líneas en emisión de treinta y tres nebulosas planetarias. Los objetos observados se encuentran a diferentes distancias del centro de la galaxia, cubriendo un rango de 10 kpc. Las observaciones se analizan para obtener información tanto de los objetos individuales como de nuestra galaxia. La composición química para una nebulosa planetaria típica de la vecindad solar es: H = 12.00, He = 11.04, C = 9.5, N = 8.33, O = 8.87 y Ne = 8.28; estos valores se refieren al logaritmo del número de átomos. Esto es, las abundancias con respecto al hidrógeno, helio, oxígeno y neón son similares a las de la Nebulosa de Orión mientras que las de carbono y nitrógeno son mayores por factores de 9 y 4, respectivamente.

Las abundancias de estos objetos indican la presencia de gradientes a lo largo del plano de la galaxia. Los valores de estos gradientes en la vecindad solar son $d\log(He/H)/dR = -0.02$ kpc^{-1}, $d\log(O/H)/dR = -0.06$ kpc^{-1} y $d\log(N/H)/dR = -0.18$ kpc^{-1}.

Los objetos observados muestran un cociente de enriquecimiento de helio a elementos pesados $\Delta Y/\Delta Z = 2.4$. Al comparar la densidad electrónica obtenida a partir de las líneas prohibidas con la densidad obtenida mediante el flujo total en Hα se encuentra que, en promedio, en las nebulosas planetarias ópticamente transparentes el volumen ocupado es 0.05 del volumen aparente.

ABSTRACT

Photoelectric spectrophotometry of emission lines in the 3400-7400Å range is presented for thirty-three planetary nebulae, covering a galactocentric radial range of about 10 kpc. These observations are analyzed to obtain information about individual objects and our galaxy. The logarithmic abundances by number of a typical planetary nebula of the solar neighborhood are H = 12.00, He = 11.04, C = 9.5, N = 8.33, O = 8.87 and Ne= 8.28. The He/H, O/H and Ne/H abundance ratios are very similar to those of the Orion Nebula while the C/H and N/H abundance ratios are larger by factors of nine and four, respectively. The abundance gradients evaluated at the solar vicinity are $d\log(He/H)/dR = -0.02$ kpc^{-1}, $d\log(O/H)/dR = -0.06$ kpc^{-1} and $d\log(N/H)/dR = -0.18$ kpc^{-1}. A relative helium to heavy element enrichment, $\Delta Y/\Delta Z$, of 2.4 is obtained. By comparing the electron density derived from forbidden lines to that derived from the total observed flux at Hα an average filling factor of 0.05 is found for the optically thin planetary nebulae in our sample.

Key words: PLANETARY NEBULAE — ABUNDANCES — CHEMICAL EVOLUTION — ABUNDANCE GRADIENTS.

* Visiting Astronomer, Cerro Tololo Inter-American Observatory and Kitt Peak National Observatory, which are operated by the Association of Universities for Research in Astronomy, Inc., under contract with the National Science Foundation.

I. INTRODUCTION

Planetary nebulae, PN, are useful tools to study the chemical evolution of the galaxy. It is possible to observe them at large distances and therefore to investigate the presence of chemical abundance gradients across the galactic disk. It is possible to gather information on two different problems: *a*) the effect that their own internal evolution produces in the composition of the ejected envelope, and the coresponding enrichment of the interstellar medium, and *b*) the composition of the interstellar medium at the time of formation of the parent star (for those elements not affected by PN stellar evolution).

Peimbert and Torres-Peimbert (1971*a*, *b*) based on photoelectric observations of PN and H II regions found that while PN shells showed a nitrogen enrichment by factors from 3 to 5, their He/H and O/H ratios were very similar to those of H II regions. Moreover D'Odorico *et al.* (1976) based on the observations of PN by Peimbert and Torres-Peimbert found very pronounced abundance gradients of O, N and He across the disk of our galaxy.

To further our knowledge of these problems, we decided to obtain observations of a large group of PN. In particular, great efforts were made to observe objects previously reported as helium rich.

In §II we describe the observational material. In §III we derive the electron temperatures, the electron densities and the distances. In §IV the chemical abundances are obtained and compared to other studies. In §V we discuss the abundance gradients at the solar neighborhood, derived from PN, as well as some aspects of the chemical evolution of our galaxy.

II. OBSERVATIONS

The observations were carried out in 1973-1975 at CTIO with the 0.91 m and 1.5 m telescopes and at KPNO with a 0.91 m telescope, as well as the Harvard scanners. Eight objects were also observed at KPNO with the 2.1 m telescope and the Image Intensifier Dissector Scanner, IIDS.

The observational procedure followed with the Harvard scanners has been described before (Peimbert and Torres-Peimbert 1974, 1976). Each object was observed two or more nights at all wavelengths listed in Table 1. The cells employed in both beams were FW-130 (S20 surface). The data were reduced by means of the calibration by Hayes and Latham (1975) which is very similar, within 3% in most wavelengths, to those of Hayes (1970) and Oke and Schild (1970).

The IIDS is a dual-beam multichannel spectrometer and was used at the 2.1 m telescope with the Gold image tube spectrograph and the Wynne camera. It has a cooled RCA glass, 3-stage magnetically focused image tube which has an S-20 photocathode and a P-11 (blue) phosphor. The two spectra are scanned by an ITT image dissector tube whose scanning aperture is $50\mu \times 250\mu$ in size, where the first number is along and the second perpendicular to the dispersion. Each spectrum of about 20 mm is recorded into 1024 channels.

Two gratings were used to cover the wavelength range of interest, one for λλ3500-5200 at a dispersion of 86Å/mm and the other for λλ4700-7800 at a dispersion of 157Å/mm. The resolution was of 16-18Å for the "red" setting and of 8-9Å for the "blue" setting.

Each object was observed typically for 20 minutes divided in four measurements, alternating the two slits. Measurements of the sky were obtained at the same time with the other slit. Observations of clear sky were made in both slits when observing extended objects where both slits were illuminated by the object. Each beam was treated independently and in all cases the sky was subtracted from the source. The sensitivity of the system for all wavelengths was determined primarily from measurements of standard stars. In addition, some PN and H II regions observed with the IIDS and the Harvard scanners were used as secondary standards. The standard stars were Feige 34, Feige 15 and Hiltner 102 calibrated by Stone (1974) and slightly modified by means of the new calibration by Hayes and Latham (1975). The continuum contribution to each emission line was substracted by interpolating the continuum at both sides of the emission line. Due to the resolution of the system λλ6717, 6731, and λλ6548, 6563, 6584 were partly blended; the line intensities of these individual lines were estimated by deconvoluting the line blends.

In Table 1 we present the intrinsic line intensities in erg cm^{-2} s^{-1}, $I(\lambda)$, given by

1977RMxAA...2..181T

LINE INTENSITIES

λ	Ident.	f(λ)	IC 351	IC 2003	NGC 1535	IC 418	NGC 2022	IC 2149	IC 2165	NGC 2371-2a
3425	[Ne V]	+.400	...	...	...	...	...	...	-0.26:	...
3726+3729	[O II]	+.315	-0.97	-0.50	-0.97	+0.21	-1.14	-0.06	-0.25	-0.42
3798	H 10	+.290	-1.27	-1.25	...	...	-1.30	-1.49*	...	-1.21
3835	H 9	+.280	-1.13	-1.09	...	...	-1.17	-1.32*	...	-1.11
3869	[Ne III]	+.270	+0.00	-0.10	-0.03	-1.56	-0.36	-0.62	+0.00	-0.16
3889	HeI+H8	+.265	-0.76	-0.80	...	...	-0.96	-0.80*	...	-0.90
3967+3970	[Ne III]+H7	+.235	-0.39	-0.45	...	...	-0.53	-0.70*	...	-0.44
4026	He I	+.225	...	...	...	...	...	-1.81	...	...
4069+4076	[S II]	+.210	...	-1.76	...	-1.54	...	-2.25	...	-1.46
4098+4102	N III +Hδ	+.200	-0.59	-0.61	-0.55	-0.59	-0.58	-0.63*	-0.57	-0.52
4267	C II	+.155	...	...	...	...	-1.99:	-2.12	...	...
4340	Hγ	+.135	-0.34	-0.35	-0.32	-0.34	-0.34	-0.34	-0.33	-0.30
4363	[O III]	+.130	-0.84	-0.95	-0.87	-2.04	-0.88	-1.48	-0.67	-0.88
4388	He I	+.125	...	...	...	...	...	-2.41	...	...
4472	He I	+.105	-1.52	-1.56	...	-1.40	-2.18	-1.47	-1.32	-1.86
4686	He II	+.045	-0.40	-0.25	-0.83	...	+0.05	...	-0.38	+0.04
4711+4713	[Ar IV]+He I	+.035	-1.17	-1.27	...	...	-0.75	...	...	-0.65
4725	[Ne IV]	+.030	...	...	...	...	...	...	...	...
4740	[Ar IV]	+.030	-1.24	-1.40	...	...	-0.92	...	...	-0.88
4861	Hβ	+.000	+0.00	+0.00	+0.00	+0.00	+0.00	+0.00	+0.00	+0.00
4922	He I	-.015	...	...	...	...	...	-2.03	...	...
4959	[O III]	-.020	+0.62	+0.57	...	...	+0.29	+0.18	...	+0.37
5007	[O III]	-.030	+1.11	+1.06	+1.07	+0.23	+0.78	+0.67	+1.08	+0.86
5198+5200	[N I]	-.075	...	...	...	-2.53	...	-2.36	...	-2.16:
5411	He II	-.115	-1.47	-1.33	...	...	-1.00	...	...	...
5518	[Cl III]	-.140	...	...	...	...	{ -1.95	...	...	{ -1.49
5538	[Cl III]	-.145	...	...	...	...		...	...	
5755	[N II]	-.190	...	...	...	-1.69	...	-2.34	-2.29:	-1.83
5876	He I	-.210	-1.10	-1.24	-0.96	-0.96	...	-1.06	-0.93	...
6300	[O I]	-.285	...	{ -1.84	...	{ -1.84	...	{ -2.15	-1.45	{ -1.15
6311	[S III]	-.290	...		...	-2.03	...		-1.73	
6363	[O I]	-.300	...	...	...	...	...	...	...	-1.88
6563	Hα	-.335	+0.43	+0.45	+0.45	+0.45	+0.46	+0.44	+0.44	+0.45
6584	[N II]	-.340	...	-0.69:	...	+0.17	< -0.84	-0.39	-0.31	-0.03
6678	He I	-.360	...	...	...	-1.53	...	-1.51	-1.47	...
6717	[S II]	-.370	...	{ -1.64	...	{ -1.23	...	-2.05	{ -1.17	{ -0.56
6731	[S II]	-.370	...		...		...	-1.80		
7006	[Ar V]	-.395	...	...	...	...	-1.44	...	...	...
7065	He I	-.400	...	-1.65	...	-1.27	...	-1.37	-1.31	...
7136	[Ar III]	-.410	-1.18	-1.06	-1.15	-1.18	-1.05	-1.07	-1.02	-0.72
7320+7330	[O II]	-.435	...	-1.44	...	-0.70	...	-1.15	-1.16	-1.31

1977RMxAA...2..181T

TABLE 1 (continued)

λ	NGC 2371-2b	M1-14	NGC 2392	NGC 2438	NGC 2440	NGC 2452	NGC 2610a	NGC 2610b	IC 2448	NGC 2792
3425	+0.28	...	...	...	...	...	...	...	...	-0.17:
3726+3729	-0.44	+0.29	+0.02	+0.50:	+0.29	-0.17:	-1.27:	-1.26:	-1.20	-0.85:
3835	...	...	...	...	...	...	-1.18:	...	...	...
3869	-0.25	-1.05	+0.08	-0.01:	+0.10	+0.00:	-0.57	-0.74:	-0.03	-0.17
3889	...	...	...	...	...	...	-0.95	...	...	...
3967+3970	...	...	...	...	...	...	-0.60	...	...	...
4069+4076	...	...	...	...	-1.41	...	...	...	...	...
4098+4102	-0.59	-0.62	-0.58	-0.60:	-0.50	-0.47:	-0.57	-0.53:	-0.54	-0.60
4340	-0.33	-0.32	-0.34	-0.35:	-0.33	-0.31:	-0.32	-0.35:	-0.34	-0.32
4363	-0.77	-1.67	-0.53	-1.02:	-0.58	-0.76:	-0.98	-0.99:	-0.77	-0.70
4472	...	-1.38	...	...	-1.36:	...	...	-1.90:	-1.38	...
4686	-0.04	...	-0.31:	-0.38	-0.25	-0.11	+0.00	-0.06:	-0.42	-0.04
4711+4713	...	...	...	...	...	...	-0.82	...	...	...
4740	...	...	...	...	...	...	-1.09	...	...	...
4861	0.00	0.00	0.00	0.00	0.00	0.00	0.00	0.00	0.00	0.00
4959	...	...	...	...	...	...	+0.08	...	...	...
5007	+0.91	+0.44	+1.10	+1.04	+1.19	+1.11	+0.56	+0.59:	+1.07	+1.03
5411	...	...	...	...	...	...	-1.11	...	...	...
5518	...	...	-1.79:	...	...	...	...	...	...	...
5755	...	-1.84:	...	...	-0.72	...	...	...	...	...
5876	...	-0.89	-1.21:	-1.12	-0.90	-1.28:	...	-1.52:	-1.00	-1.40:
6300	...	-1.45:	...	-0.78:	-0.55	...	...	...	...	...
6311	...	-1.97	-1.80	-1.58:	-1.57	...	...	...	...	...
6563	+0.46	+0.45	+0.47	+0.42	+0.44	+0.47	+0.44	+0.42:	+0.45	+0.47
6584	-0.34	-0.07	-0.01	+0.24	+1.06	-0.01	<-0.86	...	-1.58	-1.35
6678	...	-1.49	...	...	-1.41:	...	...	...	-1.64:	...
6717+6731	-0.80	-1.38:	-0.84	-0.37:	-0.46	-0.53	<-2.10	...	-2.25:	<-1.70
7006	...	...	...	...	-1.30:	...	-1.54:	...	...	...
7065	...	-1.33	...	...	-1.44	...	...	...	-1.66:	...
7136	-0.72	-1.09	-0.89	-0.75:	-0.50	-0.48	-1.32:	...	-1.25:	-0.97
7320+7330	...	-0.77	-1.26	-1.10:	-0.71	-1.25:	...	...	-1.71:	...

1977RMxAA...2..181T

TABLE 1 (Continued)

λ	NGC 3211	NGC 3242	NGC 3587a	NGC 3587b	NGC 3587c	NGC 3587d	NGC 3587e	NGC 3918	NGC 4361a
3425	-0.11:	-1.57:	...	...	...	...	...	...	+0.35:
3726+3729	-0.51	-1.05	+0.30	+0.41	+0.72	+0.40	+0.70	-0.22	-1.09:
3869	-0.04	-0.03	-0.14	-0.07	-0.08	-0.09	-0.01	+0.04	-0.59:
3889	...	...	...	-0.84	...	-0.71	...	...	...
3967+3970	...	...	...	-0.42	...	-0.40	...	...	...
4069+4076	...	...	...	...	-0.83	...	...	-1.47	...
4098+4102	-0.57	-0.56	-0.58	-0.56	-0.58	-0.57	...	-0.56	-0.54:
4340	-0.34	-0.34	-0.37	-0.29	-0.32	-0.30	...	-0.34	-0.30:
4363	-0.60	-0.84	-1.15	...	...	...	...	-0.69	-1.04:
4472	...	-1.42	...	...	...	...	...	-1.43	...
4686	-0.08	-0.42	-0.79:	-0.58	-0.91:	-0.73	...	-0.36	+0.12:
4711+4713	...	-1.24:	...	...	...	...	...	-1.10	...
4740	...	-1.29:	...	...	...	...	...	-1.09	...
4861	0.00	0.00	0.00	0.00	0.00	0.00	0.00	0.00	0.00
4959	...	...	...	+0.49	+0.45	+0.48	+0.35	...	...
5007	+1.16	+1.09	+0.92	+0.96	+0.90	+0.94	+0.81	+1.20	+0.46:
5198+5200	...	-2.55:	...	...	...	...	...	-2.25:	...
5518	...	-1.89	...	...	...	...	...	...	...
5755	...	...	...	...	...	...	...	-1.97	...
5876	-1.31	-1.00	-0.88:	-0.96:	...	...	...	-1.00	<-1.70
6300	...	...	...	...	...	...	...	-1.39	...
6311	...	...	...	...	...	...	...	-1.59	...
6563	+0.46	+0.47	+0.44	+0.46	+0.46	...	...	+0.45	+0.47:
6584	-0.80	-1.49	+0.03	+0.08	+0.51	...	...	-0.15	-1.70:
6678	...	-1.57:	...	...	...	...	...	-1.61	...
6717	...	{-2.20	-0.66	{-0.58	{-0.19	...	...	-1.60	...
6731	...		-0.85			...	...	-1.34	...
7006	...	...	...	...	...	...	...	-1.66	-1.25:
7065	...	-1.58	...	...	...	...	...	-1.39	...
7136	-0.84:	-1.14	-0.92	-0.90	...	...	...	-0.74	-1.61:
7320+7330	...	-2.02:	...	...	...	...	...	-1.11	...

1977RMxAA...2..181T

TABLE 1 (Continued)

λ	NGC 4361b	NGC 4361c	NGC 5307	NGC 5315	He2 -108	IC 4406	NGC 5882	HD 138403	HD 141969
3726+3729	<-1.50	...	-0.87:	-0.32	+0.14:	+0.66:	-0.81:	-0.11:	-0.44:
3835	-1.12	...	...	...	...	...	...	...	...
3869	-0.63	-0.60	+0.05	-0.22	-1.33:	+0.13:	-0.10:	<-2.14	<-1.19
3889	-0.96	-0.95	...	...	...	...	...	...	...
3967+3970	-0.63	-0.60	...	...	...	...	...	...	...
4069+4076	...	...	...	-1.10	...	...	...	-1.21:	-1.37:
4098+4102	-0.55	-0.56	-0.57	-0.58	-0.64:	-0.52:	-0.60:	-0.58:	-0.63:
4340	-0.32	-0.30	-0.35	-0.32	-0.37:	-0.31:	-0.35:	-0.32:	-0.36:
4363	-1.14	-0.97	-0.77	-1.39	-1.95:	-1.03:	-1.26:	...	...
4472	...	...	...	-1.20	-1.17:	-1.19:	-1.22:	...	...
4686	+0.04	+0.07	-0.55	-1.57	...	-1.05:	-1.50:	-2.15:	...
4711+4713	-0.94	-0.73	...	-1.98:	...	...	-1.48:	...	...
4725	-1.52	...	...	...	...	...	...	...	...
4740	-1.20	-0.97	...	-2.55:	...	...	-1.47:	...	...
4861	0.00	0.00	0.00	0.00	0.00	0.00	0.00	0.00	0.00
4959	-0.18	+0.05	...	...	...	...	...	...	...
5007	+0.29	+0.51	+1.11	+0.88	+0.30:	+1.09:	+1.00:	-1.33:	-1.42:
5198+5200	...	...	...	-2.09:	...	...	-2.64:	...	...
5518	...	...	...	-2.64:	...	...	-2.37:	...	...
5538	...	...	...	-2.11:	...	...	-2.31:	...	...
5755	...	...	...	-1.27	...	-1.26:	-2.75:	-1.62:	...
5876	...	...	-0.97	-0.74	-0.77:	-0.79:	-0.81:	-1.37:	...
6300	...	...	...	-1.25	...	-0.50:	...	-1.69:	-1.95:
6311	...	...	...	-1.41	...	-1.48:	-2.00:	...	...
6563	...	...	+0.46	+0.48	+0.47:	+0.45:	+0.47:	+0.45:	+0.44
6584	...	...	-1.22	+0.28	+0.02:	+0.60:	-0.87:	+0.44:	+0.29
6678	...	...	-1.58:	-1.30	-1.41:	-1.30:	-1.35:	-1.80:	...
6717	...	...	{-1.50	-1.39	...	{-0.64:	{-1.57:	-1.34:	{-0.39
6731	...	...		-1.06	...			-1.01:	
7065	...	...	-1.54:	-1.07	...	-1.50:	-1.25:	-1.72:	...
7136	...	...	-1.16:	-0.52	...	-0.55:	-0.79:	-1.58:	...
7320+7330	...	...	-1.62:	-0.87	-1.28:	-0.90:	-1.70:	-1.15:	-1.76:

1977RMxAA...2..181T

TABLE 1 (continued)

λ	PB-4	NGC 2818	IC 2501	NGC 3132a	NGC 3132b	NGC 3132c	NGC 3132d	NGC 3132e	PB-6
3726+3729	-0.74:	+0.47	-0.20	+0.50	+0.57	+0.64	+0.95:	+0.94:	-0.09
3869	-0.11:	+0.23	-0.20	-0.06:	+0.03	+0.01	-0.08:	+0.07:	+0.03
4098+4102	-0.57:	-0.62:	-0.59	...	-0.58	-0.60	-0.59:	...	-0.61
4340	-0.29:	-0.38:	-0.34	...	-0.33	-0.31	-0.29:	-0.40:	-0.34
4363	-1.19:	-0.64	-1.29	...	-1.28	-1.28	-1.38:	...	-0.76
4472	...	...	...	...	-1.27	-1.22	-1.17:	...	...
4686	-0.67:	-0.12	-2.05:	-0.58:	-0.88	-1.33	...	...	+0.06
4861	0.00	0.00	0.00	0.00	0.00	0.00	0.00	0.00	0.00
5007	+0.89:	+1.04	+0.90	+0.99	+0.94	+0.96	+0.72:	+0.68:	+0.99
5755	...	-0.85:	-1.90:	...	-1.26	-1.14	-0.90:	-1.06:	-1.21
5876	-0.80:	...	-0.82	-0.77	-0.81	-0.78	-0.67:	-0.75:	-1.01:
6300	...	...	-1.33	-0.81	-0.51	-0.66	-0.33:	-0.21:	...
6311	...	...	-2.00:	...	-1.46	-1.22	...	...	...
6563	+0.48:	+0.44	+0.44	+0.46	+0.43	+0.43	+0.45:	+0.46:	+0.45
6584	-1.01:	+0.72	-0.19	+0.64	+0.66	+0.71	+1.00:	+0.97:	+0.39
6678	...	...	-1.36	...	-1.38	-1.34	...	...	...
6717+6731	-1.48:	-0.10	-1.24	-0.08:	-0.08	-0.08	+0.17:	+0.30:	+0.02:
7065	-1.41:	...	-1.06	...	-1.50	-1.38	-1.07:	-0.79:	...
7136	-0.91:	-0.68	-0.78	-0.51:	-0.60	-0.61	-0.50:	-0.59:	-0.93
7320+7330	-1.12:	...	-0.97:	-0.99	-0.94	-1.00	-0.69:	-1.00:	-1.24

NOTES TO TABLE 1

NGC 1535. Slit 5″ N of central star.
NGC 2149. Marked intensities have not been corrected for stellar underlying absorption.
NGC 2371–2. SW region. (a) and (b) are at same position.
NGC 2452. Northern condensation.
NGC 2610. (a) and (b) are at same position.
NGC 2818. Southern region.
NGC 3132. (a) slit on central star, (b) 9″ N of a, (c) 18″ N of a, (d) 27″ N of a, (e) 36″ N of a.
NGC 3242. Slit 3″ N of central star.
NGC 3587. (a) and (b) slit on central star, (c) 94″ W of b, (d) 50″ S of b, (e) 94″ W of d.
NGC 4361. (a) slit 3″ S of central star, (b) 4″ S of central star, (c) 25″ S of central star.
HD 138403. There might be some contribution to the He and H lines from emission of a high density region closer to the star. This could be particularly the case for λ4686.

$$\log I(\lambda)/I(H\beta) = \log F(\lambda)/F(H\beta) + C(H\beta)f(\lambda). \quad (1)$$

where $F(\lambda)$ is the observed line flux corrected for atmospheric extinction and $C(H\beta)$ is the logarithmic reddening correction at $H\beta$. The reddening function, $f(\lambda)$, normalized at $H\beta$ is derived from the normal extinction law (Whitford 1958) and is also presented in Table 1. $C(H\beta)$ was determined by fitting the observed Balmer decrement to the one computed by Brocklehurst (1971) for $T_e = 10000$ °K and $N_e = 10000$ cm^{-3} and is presented in column 5 of Table 2. The hydrogen Balmer line intensities presented in Tables 1 and 2 have not been corrected for the He^+ Pickering emission line contribution. Alternatively, λ6678 has been corrected from the contribution due to Pfund 13 of HeII (λ6683), based on the observed intensity of λ4686 and the theoretical computations by Brocklehurst.

By comparing the intrinsic Balmer line ratios presented in Table 1 and the theoretical ones computed by Brocklehurst (1971), as well as the line intensity ratios derived in different nights, it is estimated that the logarithmic rms errors are smaller than 0.04 for the objects observed with the Harvard scanners and 0.06 for the objects observed with the IIDS. The intensities listed with a colon present rms errors twice as large.

In Table 2 we present our observations of the flux and the reddening correction at $H\beta$ as well as a description of the instrument and aperture used. The observed flux at $H\beta$ (column 2), the logarithmic reddening correction (column 4), and the line intensities given in Table 1 were observed with the listed telescope (column 5) and entrance slit (column 6). The entrance slits were always oriented east-west. In general, the entrance slit used does not include the whole object. Our observed flux for the whole object, when available, is listed (column 3). For comparison, we include the flux obtained by other authors, as well as the corresponding reference (columns 7 and 8). The determinations by Webster (1969) are in excellent agreement with our observations. The absolute calibration of α Lyrae adopted by Hayes and Latham (1975) is 0.03 fainter in log $F(H\beta)$ than the value by Code (1960) which was used by Webster and the Wisconsin group.

In addition to the observations presented here, we will rediscuss the observations of Peimbert *et al.* (1971*a*); therefore our total sample will be of 42 objects, which are listed in Table 4 and subsequent tables. Two objects were observed independently in both surveys. The objects with an asterisk in Table 4 are the best observed PN, the intensities given are of higher accuracy, and in general more lines were measured for them. The best observed objects are marked by crosses in Figures 3-5 and 7-11. Since we will be referring to the observations by Peimbert et al. (1971*a*) we would like to point out that there are two errata in it: *a*) For IC 5217 the published intrinsic line ratio, $\log I(5876)/I(H\beta)$, should be −0.94 instead of −0.80; *b*) In equation (1) instead of $-2 \ln Z$ it should read $-\ln Z$ (also equations (2) and (8) should be corrected); this is a very insensitive term and it does not affect the results presented in that paper.

III. BASIC PARAMETERS

a) *Electron temperatures and densities derived from forbidden lines*

The references to the atomic parameters used to derive electron temperatures, electron densities and chemical abundances are presented in Table 3. The collision strengths for S^+ correspond to computations made in the distorted wave single configuration and correlation approximation. The accuracy of the collision strengths for N^+, O^+, O^{++} and Ne^{++} is probably of 5% and better than 10% (Seaton 1975). For the other ions the errors could be considerably larger.

We computed the dependence on temperature and density of the forbidden line intensity ratios and obtained solutions in the (N_e, T_e) diagram for the available ratios. Two sample diagrams are presented in Figure 1. In the case of a homogeneous nebula of uniform temperature and density all the curves in the (N_e, T_e) diagram should intersect in only one point. This is not the case and in what follows we will discuss a two zone scheme to compute chemical abundances.

We will use the temperature T(N II), given by the $I(5755)/I(6584)$ ratio and N_e(FL) (see below), as representative of the regions of low degree of ionization where the [S II], [O II] and [N II] lines

TABLE 2

OBSERVED FLUX AND REDDENING CORRECTION. TELESCOPE AND ENTRANCE SLIT USED.

Object	This paper					Other authors	
	log F(Hβ)*	log F(Hβ)† (whole object)	C(Hβ)	Telescope	Slit‡	log F(Hβ) (whole object)	Ref.§
IC 351	-12.49	...	0.4	2.1KP	D	-11.43	O62
IC 2003	-12.17	...	0.4	2.1KP	D	-11.21	O63b
NGC 1535	-11.13	...	0.1	0.9CT	A	-10.39	O62
IC 418	-10.10	- 9.52	0.35	0.9CT	A	- 9.56	O62
NGC 2022	-12.31	...	0.6	2.1KP	D	-11.18	O63b
IC 2149	-11.29	...	0.3	2.1KP	D	-10.53	O62
IC 2165	-11.20	-10.90	0.5	0.9CT	A	-11.03	O62
NGC 2371-2a	-12.39	...	0.1	2.1KP	E	-10.99	O62
NGC 2371-2b	-11.57	...	0.1	0.9KP	C	...	...
M1-14	-11.55	-11.55	0.85	1.5CT	F	...	...
NGC 2392	-10.82	...	0.1	0.9KP	C	-10.42	O62
NGC 2438	-11.96	...	0.3	1.5CT	B	-11.05	O63b
NGC 2440	-11.03	-10.48	0.2	0.9CT	A	-10.59	O63b
NGC 2452	-12.02	...	0.5	1.5CT	B	-11.57	O63b
NGC 2610a	-12.79	...	0.1	2.1KP	E	-11.41	O63b
NGC 2610b	-12.08	...	0.1	1.5CT	B	...	...
IC 2448	-11.18	-10.84	0.15	1.5CT	B	-10.85	W69
NGC 2792	-11.78	...	0.75	1.5CT	B	-11.42	AF64
PB-4	-11.64	-11.64	0.6:	1.5CT	F	-11.66	W69
NGC 2818	-12.01	...	0.3	0.9CT	A	-11.43	O63b
IC 2501	-10.64	-10.64	0.50	0.9CT	F	...	...
NGC 3132a	-11.26	...	0.2	1.5CT	B	-10.40	W69
NGC 3132b	-11.34	...	0.2	1.5CT	B	...	...
NGC 3132c	-11.44	...	0.2	1.5CT	B	...	...
NGC 3132d	-11.88	...	0.2	1.5CT	B	...	...
NGC 3132e	-12.40	...	0.2	1.5CT	B	...	...
PB-6	-12.24	-11.85	0.55	1.5CT	B	...	...
NGC 3211	-11.43	...	0.25	1.5CT	B	-11.07	W69
NGC 3242	-10.46	...	0.0	1.5CT	B	- 9.84	O62
NGC 3587a	-11.82	...	0.0	0.9KP	C	-10.36	O62
NGC 3587b	-13.23	...	0.0	2.1KP	E	...	...
NGC 3587c	-13.89	...	0.0	2.1KP	E	...	...
NGC 3587d	-13.15	...	0.0	2.1KP	E	...	...
NGC 3587e	-13.91	...	0.0	2.1KP	E	...	...
NGC 3918	-10.44	-10.03	0.30	0.9CT	A	-10.04	W69
NGC 4361a	-11.65	...	0.1	1.5CT	B	-10.51	O62
NGC 4361b	-12.54	...	0.1	2.1KP	E	...	...
NGC 4361c	-13.12	...	0.1	2.1KP	E	...	...
NGC 5307	-11.58	-11.21	0.4	1.5CT	B	-11.18	AF64
NGC 5315	-10.54	-10.42	0.6	0.9CT	A	-10.41	W69
He2-108	-11.41	-11.41	0.4	1.5CT	F	...	...
IC 4406	-11.44	...	0.3	1.5CT	B	-10.76	AF64
NGC 5882	-10.62	-10.35	0.4	1.5CT	B	-10.36	W69
HD 138403	-10.15	-10.15	0.2	0.9CT	F	-10.16	W69
HD 141969	-10.68	-10.68	0.2	0.9CT	F	-10.75	W69

* Obtained with listed telescope and entrance slit.
† Obtained with listed telescope and circular entrance diaphragm (F).
‡ (A) 4.8"x71.5" (B) 5.2"x77.6" (C) 11"x125" (D) 2"x12.2" (E) 3.5"x12.2" (F) circular, comprising object.
§ Webster 1969; O'Dell 1962; O'Dell 1963b; Aller and Faulkner 1964.

TABLE 3

REFERENCES TO ATOMIC PARAMETERS

Ion	A	Ω or Υ
N^+	Nussbaumer 1971	Seaton 1975
O^+	Seaton and Osterbrock 1957	Pradhan 1976*a*
O^{++}	Nussbaumer 1971	Eissner and Seaton 1974
Ne^{++}	Garstang 1968	Pradhan 1974
S^+	Czyzak and Krueger 1963	Pradhan 1976*b*
S^{++}	Czyzak and Krueger 1963	Czyzak *et al.* 1968
Cl^{++}	Czyzak and Krueger 1963	Conneely *et al.* 1970
Ar^{++}	Czyzak and Krueger 1963	Czyzak *et al.* 1968

originate; and T(O III), given by the I(4363)/I(5007) ratio and N_e(FL), as representative of the high degree of ionization regions. A logarithmic error of 0.04 in the observed line intensity ratios introduces errors of ~300°K in T(O III) and T(N II). In general, it is found that for objects of high degree of ionization [where log I(4686)/I(Hβ) > −0.6], T(O III) is about 1.25 times higher than T(N II); while for those of low degree of ionization, T(O III) and T(N II) are very similar. The temperatures derived from the observed ratios are presented in Table 4. For about half of the objects presented in this table I(5755) was not measured and thus we adopted T(N II) = T(O III)/1.25 for the objects of high degree of ionization; while for those of low degree of ionization we adopted T(N II) = T(O III). The adopted values are given in parentheses in Table 4.

From our data, we have as the main density indicator the [O II] auroral to nebular line ratio, I(7325)/I(3727). In the presence of spatial temperature and density fluctuations the density derived from this ratio is somewhat higher than that derived from the I(3726)/I(3729) nebular ratio. The nebular ratio provides a more representative value of the average density of the emitting regions (Peimbert 1971; Peimbert and Torres-Peimbert 1977).

In Table 4 we present the adopted electron densities from forbidden lines, N_e(FL); where in general we used a value 1.4 times smaller than that given by the I(3727)/I(7325), I(5755)/I(6584) intersection on the (N_e, T_e) diagram. In a few cases the nebular [S II] and [Cl III] line ratios were also used to find the average density. For the cases for which

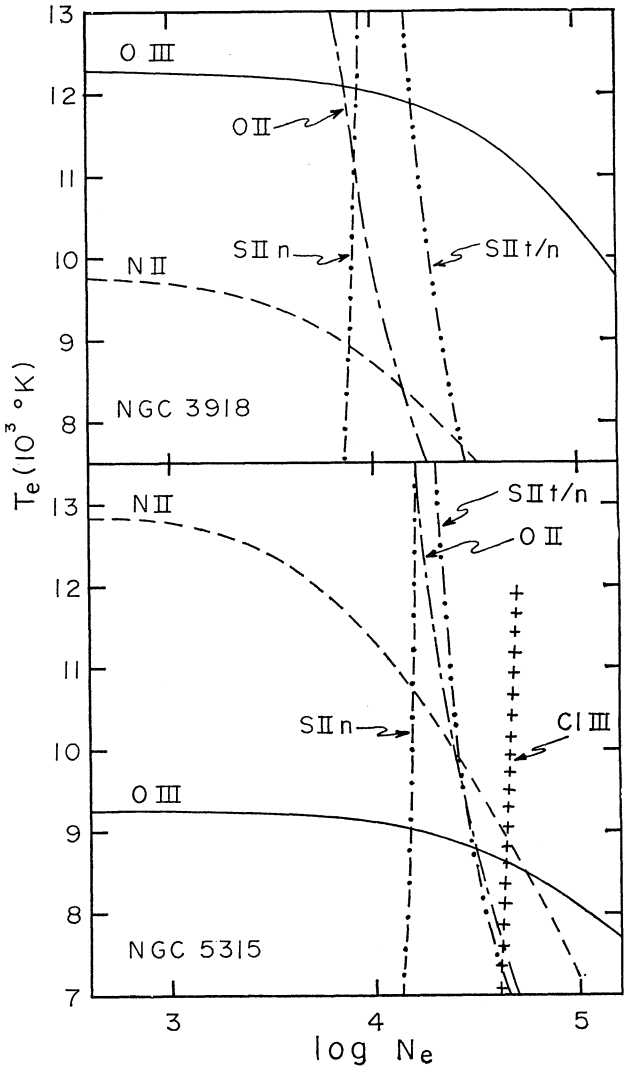

FIG. 1. Solutions of electron temperature and density for the observed forbidden line intensity ratios for NGC 3918 and NGC 5315. The observed ratios are I(4363)/I(5007) for O III; I(5755)/I(6584) for N II; I(3727)/I(7325) for O II; I(6717)/I(6731) for $S II_n$; I(4073)/I(6724) for $S II_{t-n}$; I(5518)/I(5538) for Cl III.

no line ratios sensitive to the electron density were available we used the N_e(FL) *vs.* N_e(rms) diagram (see below) to estimate N_e(FL); these values are given in parenthesis in Table 4.

In general to derive temperatures and abundances of the high density regions it is not required to know the electron density of these regions, (namely for [O III] and [Ne III]. Therefore we have used

TABLE 4

TEMPERATURE, DENSITY, DISTANCE AND SIZE

Object	T(N II)	T(O III)	N_e(FL) (10^4 cm^{-3})	N_e(rms) (10^4 cm^{-3})	d (kpc)	R (kpc)	z (kpc)	r (pc)
IC 351	(8700)	11600	(0.5)	0.14	8.12	17.7	2.13	0.14
IC 2003	(8400)	11000	0.6	0.21	7.60	17.2	1.95	0.12
NGC 1535	(11700)	11700	(0.6)	0.13	3.23	12.4	2.10	0.14
IC 418*	8300	9100	1.2	1.7	0.68	10.5	0.28	0.021
NGC 2022	(11400)	15300	(0.3)	.078	3.58	13.4	0.68	0.17
IC 2149	8200	10000	0.6	0.50	2.32	12.2	0.42	0.047
IC 2165	8000	13900	0.5	0.41	2.82	12.2	0.61	0.055
NGC 2371-2a	9600	14000	0.3	0.019	2.54	12.4	0.86	0.27
NGC 2371-2b	(11300)	15000	(0.3)	...	...	...	...	...
M1-14	9600	10300	0.5	...	3.98	12.7	0.10	...
NGC 2392	(11900)	15800	0.1	0.040	1.92	11.8	0.57	0.21
NGC 2438	(8100)	10800	0.05	0.014	1.79	11.2	0.13	0.30
NGC 2440	9700	13600	0.4	0.065	2.28	11.5	0.10	0.18
NGC 2452	(9400)	12500	0.3	0.040	4.46	12.6	0.08	0.21
NGC 2610a	(13200)	17600	(0.1)	0.013	3.30	12.0	0.80	0.31
NGC 2610b	(12600)	16800	(0.1)	...			...	...
IC 2448	(9400)	12500	1.2	0.17	5.97	10.2	1.54	0.13
NGC 2792	(10700)	14200	(0.3)	0.11	4.54	11.3	0.32	0.15
PB-4	(10300)	10300:	1.2:	0.089	6.36	11.4	0.46	0.16
NGC 2818	12500	15000	(0.1)	0.014	2.64	10.7	0.39	0.28
IC 2501*	9700	9000	1.0*†	5.2	2.09	9.8	0.21	0.010
NGC 3132b	8900	9600	0.1	.040	1.63	10.1	0.35	0.21
NGC 3132c*	9400	9400	0.1	...	...	...	...	...
NGC 3132d	9200	10500	0.1	...	...	...	...	...
NGC 3132e	8200	...	0.01	...	...	...	...	...
PB-6	11900	14000	0.2	0.057	7.01	11.3	0.61	0.19
NGC 3211	(10300)	13700	(0.5)	0.092	3.74	9.7	0.32	0.13
NGC 3242*	(8900)	11800	0.4	0.092	1.66	10.4	0.88	0.16
NGC 3587a	(10700)	10700	(0.1)	0.0073	0.84	10.4	0.70	0.37
NGC 3587c	...	...	0.4	...	...	...	...	...
NGC 3918*	8900	12100	0.9	0.46	1.30	9.5	0.11	0.05
NGC 4361a	(14000)	18600	(0.05)	0.17	1.40	9.7	0.97	0.28
NGC 4361b	(15400)	20500	(0.05)	...	...	...	...	...
NGC 4361c	(14300)	19000	(0.05)	...	...	...	...	...
NGC 5307	(9200)	12300	0.6	0.093	5.11	7.6	0.94	0.16
NGC 5315*	10900	9000	1.4	1.9	1.45	9.2	0.11	0.02
He2-108	(9400)	9400	0.2	...	5.69	7.2	0.84	...
IC 4406	9300	10300	0.1	0.047	2.42	8.4	0.66	0.20
NGC 5882	8300	9200	1.0	0.51	1.68	8.7	0.29	0.047
HD 138403	7500	(7500)	0.9	1.4	1.68	8.9	0.38	0.024
HD 141969	7300	...	(0.8)	0.42	3.09	7.9	0.52	0.052
NGC 6572*	11500	9200	2.0	1.07	0.9	9.3	0.19	0.027
IC 418*	8500	9100	1.4	1.7	0.68	10.5	0.28	0.021
NGC 6803*	9200	9200	1.0	0.52	3.48	8.0	0.25	0.047
NGC 7009*	10800	9600	0.6	0.18	1.89	8.8	1.1	0.12
NGC 7027*	11000	11000	5.0‡	2.8	0.51	10.0	0.03	0.016
BD+30°3639*	8200	(...)	1.0	1.7	1.07	9.6	0.09	0.021
NGC 6884*	(9400)	9400	1.0	0.57	2.90	10.0	0.36	0.045
NGC 7662*	(9400)	12500	0.4	0.26	1.53	10.5	0.46	0.078
IC 5217*	(10600)	10600	1.4	0.19	7.70	13.7	0.73	0.13
NGC 1535*	(11100)	11100	0.6	0.13	3.23	12.4	2.10	0.14
NGC 6720*	9700	10300	(0.1)	0.034	1.26	9.5	0.31	0.21

* Best observed objects

† N_e(FL,high)= 5×10^4

‡ N_e(FL,high)=16×10^4

the N_e(FL) values derived from the low density regions as representative of the whole object.

There are two exceptions to this, NGC 7027 and IC 2501. For these objects we used a two density scheme: one density for the regions of low degree of ionization, N_e(FL, low) and another density for the regions of high degree of ionization, N_e(FL, high). For IC 2501, from the forbidden line observations we find log N_e(FL, low) = 4.0 and due to the very large N_e(rms) value (see below) we will adopt log N_e(FL, high) = 4.7. For NGC 7027, from our observations, we derive log N_e(FL, low) = 4.7 while for log N_e(FL, high) we will adopt a value of 5.2 (Saraph and Seaton 1970; Goad *et al.* 1972; Kaler *et al.* 1976).

b) *Distances*

The Shklovsky (1956) method has been used extensively to determine distances to planetary nebulae (cf. O'Dell 1962, 1963*a*, 1968; Seaton 1966, 1968*b*; Webster 1969; Cahn and Kaler 1971: Osterbrock 1973; Cudworth 1974). This method applies to optically thin PN and is based on the assumptions that the ejected mass is: *a*) the same for all the objects and *b*) adequately represented by the root mean square mass, M(rms). We will come back to these assumptions in §III*d*. The two most recent calibrations of this distance scale are those by Seaton (1968*b*) and Webster (1969) and by Cudworth (1974). Seaton based his calibration on the assumption that the brightest planetary nebulae in the LMC and in the solar vicinity are optically thick, while Cudworth (1974) based his calibration on statistical parallaxes. From the use of his distance scale Cudworth finds that the brightest PN in the solar neighborhood are optically thin.

In what follows we use for the optically thin objects the distance scale by Cudworth. It is 1.5 times larger than that by Seaton and Webster, and is given by

$$d = 108\,\phi^{-3/5}\,I(H\beta)^{-1/5}\ \text{pc}, \qquad (2)$$

where ϕ is the angular radius in arc sec. For the radius we used the average of the values quoted in Cahn and Kaler (1971) or in the Catalogue by Perek and Kohoutek (1967). We defined as optically thin all those objects for which the radius turned out to be larger than 0.12 pc using the optically thin distance scale.

To obtain the distance to the optically thick PN we have followed the proposal by Minkowski (1965); that is, to assume that the number of ionizations per second is the same for all objects. Again, based on statistical parallaxes, Cudworth (1974) has calibrated the distance scale for the optically thick case to be

$$d = 0.0178\,I(H\beta)^{1/2}\ \text{pc}. \qquad (3)$$

This calibration is very similar to that derived previously by Minkowski. The distances derived from equations (2) and (3) are presented in Table 4. The radius, r, the galactocentric distance, R, and the height above the plane, z, for each object are also presented in Table 4.

c) *Electron densities derived from Hβ fluxes*

The intrinsic Hβ flux observed from a homogeneous sphere of radius r is given by

$$I(H\beta) = \frac{N_e(\text{rms})\,N_p(\text{rms})\,r^3\,a(4\to 2, T)\,h\nu(4\to 2)}{3d^2}, \qquad (4)$$

where $a(4\to 2, T)$ is the Hβ effective recombination coefficient and N_e and N_p are the electron and proton rms densities.

From (4) we have

$$N^2_e(\text{rms}) = \frac{3d^2\,I(H\beta)\left[1+\frac{N(He^+)}{N(H^+)}+\frac{2N(He^{++})}{N(H^+)}\right]}{r^3\,a(4\to 2, T)\,h\nu(4\to 2)}. \qquad (5)$$

From the value of a for T = 10000°K by Brocklehurst (1971) and the helium to hydrogen abundance ratios given in Table 5, the N_e(rms) values presented in Table 4 were derived.

d) *Filling factor and mass*

In the case of a homogeneous distribution of mass N_e(FL) = N_e(rms), the mass of the emitting envelope of a PN is given by

$$M(\text{rms}) = \langle m\rangle\,N_e(\text{rms})\,V, \qquad (6)$$

where V is the emitting volume and ⟨m⟩ is the mean atomic mass per free electron.

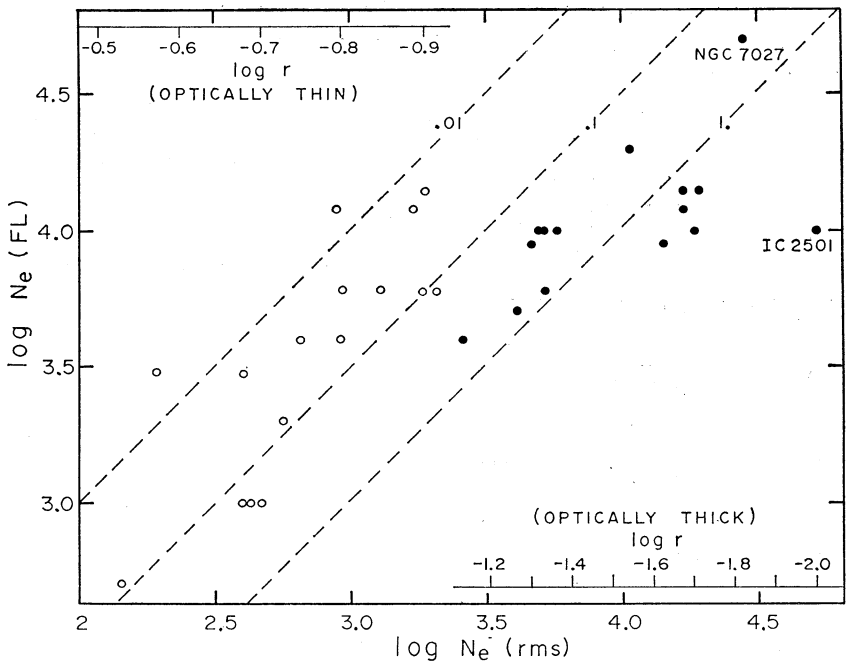

FIG. 2. Comparison between the electron density derived from forbidden line ratios, $N_e(FL)$, and that derived from $I(H\beta)$, $N_e(rms)$. Broken lines correspond to filling factors of 0.01, 0.1 and 1.0. The scales for radii of the nebulae (in parsecs) are given for the optically thin and optically thick cases.

The Cudworth distance scale for optically thin PN yields $M(rms) = 0.50\,M_\odot$. However, from the values presented in Table 4 (see also Figure 2), in most objects $N_e(FL) > N_e(rms)$, implying the presence of density fluctuations. To reconcile both densities it is possible to adopt a model of extreme density fluctuations in which a fraction α of the volume is filled with the high density $N_e(FL)$ and the rest is practically empty, such that,

$$N^2_e(rms) = \alpha\, N^2_e(FL). \qquad (7)$$

For this model the mass is given by

$$\begin{aligned} M(\alpha) &= \langle m\rangle N_e(FL)\alpha\, V \\ &= \langle m\rangle\, N_e(rms)\alpha^{1/2}\, V \\ &= \alpha^{1/2}\, M(rms). \end{aligned} \qquad (8)$$

From Figure 2 the average filling factor is 0.05 which implies a mean mass of $\langle M(\alpha)\rangle = 0.11\,M_\odot$. It is clear that the fluctuations of density are not as extreme as in the adopted model, and that the real mass is comprised between $M(rms)$ and $M(\alpha)$ (for those cases where $N_e(FL)$ is representative of the high density regions). For the distance scale of Seaton (1968*b*) and Webster (1969) the mean values are $\langle M(rms)\rangle = 0.18\,M_\odot$, $\alpha = 0.075$, and $M(FL) = 0.05\,M_\odot$.

IV. CHEMICAL ABUNDANCES

To derive chemical abundances we adopted a mean square temperature fluctuation of $t^2 = 0.035$ (Peimbert and Torres-Peimbert 1977) and two different temperatures corresponding to the zones of low and high ionization degree given by T(N II) and T(O III), respectively. In §IV*c* we discuss the effect in our abundance determinations of using different values of t^2.

a) *Oxygen, nitrogen, neon, sulfur chlorine and argon*

The ionic abundance ratios are obtained from relations of the type

$$\frac{N(X^{+P})}{N(H^+)} = K(X^{+P}, N_e, T_{FL})\,\frac{T_{FL}^{1/2}}{T_{H\beta}^{0.84}} \times \frac{I(FL)}{I(H\beta)} \exp\frac{\Delta E}{kT_{FL}}, \qquad (9)$$

where the Hβ emission coefficient was obtained from Brocklehurst (1971) for case B, $N_e = 10000$ cm^{-3} and it was interpolated for the temperature range 5000 − 10000°K. The K factors were computed from Brocklehurst and the references listed in Table 3. In general the K factors are weakly dependent on the electron temperature and density. T_{FL} and $T_{H\beta}$ are given by (Peimbert and Costero 1969)

$$T_{FL}^{-1/2} \exp(-\Delta E/kT_{FL}) = T_0^{1/2} \exp(-\Delta E/kT_0) \times \{1 + \left[\left(\frac{\Delta E}{kT_0}\right)^2 - 3\frac{\Delta E}{kT_0} + \frac{3}{4}\right]\frac{t^2}{2}\}, \quad (10)$$

and

$$T_{H\beta} = T_0(1 - 1.84\ t^2/2)\ ; \quad (11)$$

where ΔE is the energy difference between the ground and the excited level where the forbidden line originates, and T_0 is the average temperature.

T_0 is related to T(N II) and T(O III) by (Peimbert 1967)

$$T_{FL/FL'} = T_0\{1 + \left(\frac{\Delta E + \Delta E'}{kT_0} - 3\right)\frac{t^2}{2}\}. \quad (12)$$

We obtained the mean temperature for the low ionization region, T_0(low) from equation (12), $t^2 = 0.035$ and $T_{FL/FL'} = T(N\ II)$. T_0(low) was used together with equations (9-11) to derive the abundances of O^+, N^+, S^+, S^{++} and Cl^{++}. Similarly, to obtain T_0(high) and the O^{++}, Ne^{++} and Ar^{++} abundances, $t^2 = 0.035$ and T(O III) were combined. The results are presented in Table 5.

To derive total chemical abundances it is necessary to estimate the fraction of atoms in the unobserved stages of ionization.

For oxygen we assumed

$$\frac{N(O)}{N(H)} = \frac{N(O^+ + O^{++})}{N(H^+)}\frac{N(He^+ + He^{++})}{N(He^+)}. \quad (13)$$

This relation is an excellent approximation for PN because, even if [O I] lines are present in some of these objects, a similar fraction of oxygen and hydrogen is expected in the neutral stage. Furthermore, the $N(He^+ + He^{++})/N(He^+)$ factor includes the fraction of oxygen atoms in higher ionization stages than the second, since the ionization potentials of O^{++} and He^+ are very similar.

The total nitrogen and neon abundance can be obtained from

$$\frac{N(N)}{N(H)} = \frac{N(N^+)}{N(H^+)}\frac{N(O)}{N(O^+)} = \frac{N(N^+)}{N(H^+)}\, i_{cf}(N) \quad (14)$$

and

$$\frac{N(Ne)}{N(H)} = \frac{N(Ne^{++})}{N(H^+)}\frac{N(O)}{N(O^{++})} = \frac{N(Ne^{++})}{N(H^+)}\, i_{cf}(Ne)\,. \quad (15)$$

These relations are based on the similarity of the first and second ionization potentials of oxygen, nitrogen and neon.

Relation (14) has been tested in the Orion Nebula, by observing many points at different distances of the exciting stars (Peimbert and Torres-Peimbert 1977), and in NGC 6720 (Hawley and Miller 1977) comprising a range in $i_{cf}(N)$ of one and two orders of magnitude, respectively. No significant point to point variations in the derived N(N)/N(H) value for these objects was found, implying that equation (14) is a valid relation. In Figure 3 we present the N/O *vs.* $i_{cf}(N)$ diagram for the observed PN. No general trend is present and the scatter is mainly due to real variations from object to object in the N/O ratio, which will be discussed in §V, and to observational uncertainties.

The observations of the Orion Nebula (Peimbert and Torres-Peimbert 1977) also confirm that relation (15) represents a good approximation for this particular object. On the other hand, there are two observational results that indicate that equation (15) is not valid for all conditions. In Figure 4 we present log Ne/O *vs.* log O^+/O. Within the accuracy of the determinations Ne/O is independent of the ionization degree for those objects of medium and high degree of ionization. Alternatively, for IC 418, a PN of low degree of ionization, the Ne/O ratio turns out ot be substantially lower than the average value. This low value of Ne/O is probably due to the presence of a region where O^{++} and Ne^+ coexist, and relation (15) is no longer a valid approximation. Since the ionization potential of Ne^+ is 41 eV while that of O^+ is 35 eV it is possible that, for relatively cool stars, the number of stellar photons more energetic than 41 eV is not enough to doubly ionize Ne^+

TABLE 5

IONIC ABUNDANCES

Object	He^+/H^+	He^{++}/H^+	log N^+	log O^+	log O^{++}	log Ne^{++}	log S^+	log S^{++}	log Cl^{++}	log Ar^{++}
IC 351	.063	.035	...	7.25	8.58	7.92	...	...	...	5.75
IC 2003	.048	.049	7.01:	8.00	8.61	7.91	5.30	...	...	5.92
NGC 1535	.078	.013	...	6.67	8.50	7.89	...	...	...	5.75
IC 418	.076	...	7.92	8.80	8.13	6.85	5.87	6.90	...	6.03
NGC 2022	.015	.105	<6.44	6.49	7.89	7.13	...	...	4.70	5.76
IC 2149	.071	...	7.34	8.38	8.37	7.57	5.39	...	...	6.02
IC 2165	.096	.037	7.47	8.23	8.35	7.61	5.87	7.29	...	5.72
NGC 2371-2a	.032	.102	7.46	7.53	8.08	7.46	6.16	...	5.26	6.04
NGC 2371-2b	...	.083	6.94	7.19	8.03	7.26	5.72	...	...	5.97
M1-14	.088	...	7.41	8.31	8.08	7.09	5.35:	6.51	...	5.95
NGC 2392	.048:	.045:	7.18	7.45	8.14	7.51	5.54	6.38	:	4.88
NGC 2438	.060	.035	7.97	8.71:	8.62	8.04:	6.50	7.41:	...	6.26:
NGC 2440	.103	.050	8.53	8.26	8.43	7.75	6.26	7.00	...	6.26
NGC 2452	.041:	.069	7.51	7.82:	8.47	7.79:	6.16	...	...	6.38
NGC 2610a	...	.093	<6.23	5.99:	7.50	6.73	<4.27	...	...	5.23:
NGC 2610b	.028:	.081:	...	6.07:	7.58:	6.62:	...	...	...	...
IC 2448	.078	.033	5.98	7.08	8.44	7.75	4.66:	...	...	5.59:
NGC 2792	.031:	.076	5.99	6.87:	8.22	7.42	<4.88	...	...	5.76
PB-4	.108:	.018:	6.42:	7.29:	8.54:	8.03:	5.31:	...	...	6.15:
NGC 2818	...	.069	7.87	7.83	8.16	7.74	6.24	...	...	6.01
IC 2501	.108	.001:	7.31	7.95	8.85	8.24	5.60	6.55:	...	6.45
NGC 3132c	.124	.004	8.20	8.52	8.78	8.36	6.59	7.40	...	6.57
PB-6	.078:	.105	7.61	7.39	8.30	7.65	6.46:	...	...	5.83
NGC 3211	.039	.078	6.62	7.38	8.41	7.62	...	...	...	5.94:
NGC 3242	.075	.033	6.11	7.12	8.54	7.85	4.63	...	...	5.77
NGC 3587a	.100:	.013:	7.25	7.90	8.50	7.92	6.06	...	...	6.09
NGC 3918	.074	.038	7.47	8.09	8.61	7.87	5.80	7.16	...	6.14
NGC 4361a	.0007	.129:	5.33:	6.08:	7.34:	6.65:	...	...	...	4.81:
NGC 4361b	...	.107	...	<5.55	7.08	6.51	...	...	...	...
NGC 4361c	...	.115	...	...	7.37	6.68	...	...	...	...
NGC 5307	.077	.025	6.35	7.27:	8.50	7.86	5.43	...	...	5.70:
NGC 5315	.120	.002	7.64	7.66	8.81	8.23	5.85	6.91	5.66:	6.71
He2-108	.117:	...	7.52:	8.07:	8.12:	7.02:	...	...	...	...
IC 4406	.126:	.007:	8.11:	8.57:	8.74:	8.27:	6.05:	7.16:	...	6.51:
NGC 5882	.110:	.003:	6.87:	7.69:	8.88:	8.30:	5.50:	6.92:	5.04:	6.41:
HD 138403	.032:	.001:	8.34:	8.64:	7.03:	<6.78	6.38:	...	...	5.94:
HD 141969	...	...	8.24	8.36:	7.01:	<7.81	6.86	...	...	...
NGC 6572	.105	.000:	7.08	7.64	8.93	8.30	5.21	...	...	...
IC 418	.072	...	7.94	8.73	8.02	6.69	...	...	...	...
NGC 6803	.112	.003	7.68	7.98	8.97	...	6.05	...	...	...
NGC 7009	.103	.011	6.56	7.05	8.88	8.32	5.06	...	...	...
NGC 7027	.076	.039	7.49	7.96	8.80	...	5.78	...	...	...
BD+30°3639	.043:	...	8.54	8.98	7.02:	...	6.64:	...	...	...
NGC 6884	.104	.013	7.21	7.77	8.98	...	5.44	...	...	...
NGC 7662	.056	.038	6.15	7.17	8.41	...	4.77	...	...	...
IC 5217	.081	.005:	6.81	7.50:	8.67	...	5.20	...	...	...
NGC 1535	.086	.010	<5.76	6.77:	8.56	...	<4.30	...	...	...
NGC 6720	.071:	.036	7.39:	...	8.56	...	5.74:	...	...	...

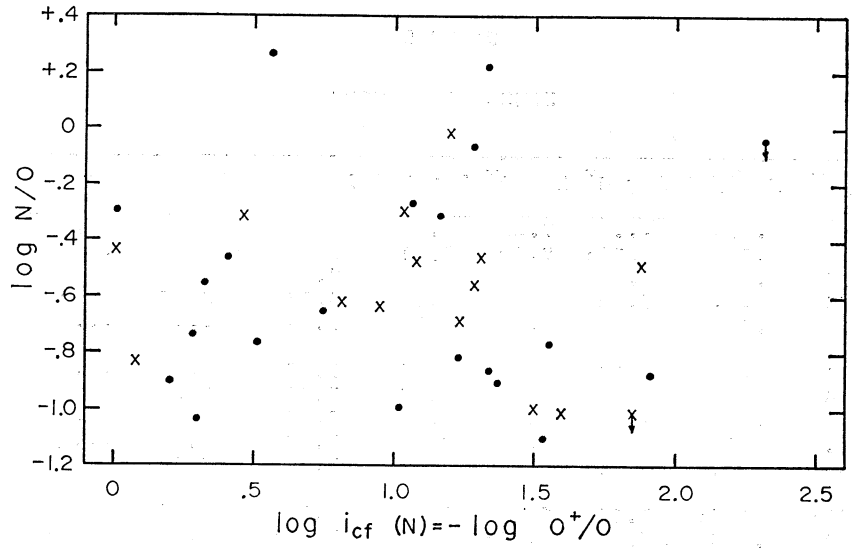

FIG. 3. Nitrogen to oxygen abundance ratio is compared to the nitrogen ionization correction factor. No systematic effects were found. Crosses are best observed objects.

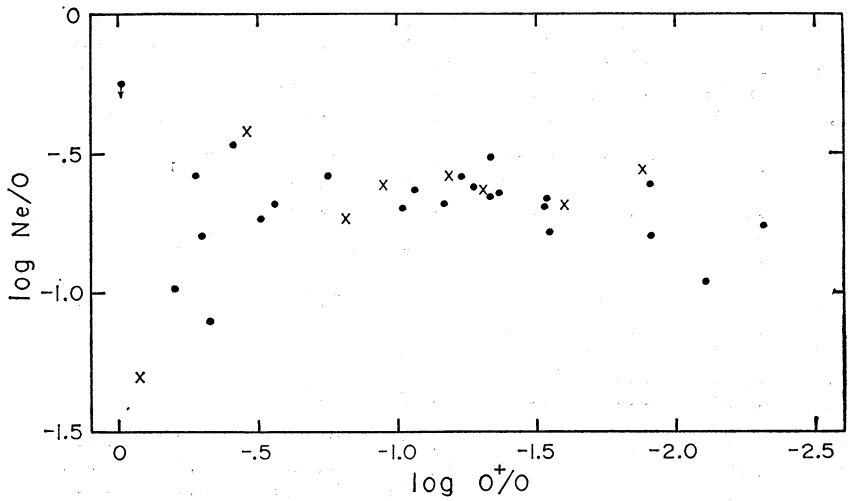

FIG. 4. Neon to oxygen abundance ratio is compared to the degree of oxygen ionization. For objects of low ionization there is a systematic deficiency of Ne, probably due to errors in the neon ionization correction factor. Crosses are best observed objects.

throughout the O^{++} region. A model of IC 418 has been computed by Flower (1969*b*) in which he discussed this problem. Moreover Balick and Sneden (1976) have computed H II region models in which this effect is also present. Since this relative lack of Ne^{++} is not present in the Orion Nebula, which is mainly ionized by an O7 star, we expect the deficiency of photons more energetic than 41 eV to be present in stars of spectral type later than O7. Therefore it will not affect the Ne/O ratio derived from equation (15) for the PN ionized by earlier type stars. Hawley and Miller (1977) find that apparently O^+ and Ne^{++} coexist in the outer edges of NGC 6720, this result should be confirmed by independent observations since at present there is no theoretical explanation for it.

b) *Helium*

The total helium to hydrogen abundance ratio in a PN is given by

$$y = y^0 + y^+ + y^{++}, \quad (18)$$

where

$$y^i = \frac{\int N_e N(He^i)\,dV}{\int N_e N(H^+)\,dV}. \quad (19)$$

In the presence of temperature fluctuations, y^+ and y^{++} can be determined directly by (Peimbert and Costero 1969)

$$y^i = KT_0^{\alpha-\beta}\{1 + \frac{1}{2}[\alpha(\alpha - 1) - \beta(\beta - 1)]t^2\}\frac{I(He, \lambda)_{rad}}{I(H, \lambda)}, \quad (20)$$

where K is constant and α and β are the power dependences on the temperature corresponding to the hydrogen and helium lines, respectively. The observed helium line intensities are related to the radiative recombination case by

$$I(He, \lambda) = I(He, \lambda)_{rad} \times [1 + \gamma_{ce}(He, \lambda) + \gamma_{sa}(He, \lambda)]; \quad (21)$$

where γ_{ce} is the collisional excitation parameter and γ_{sa} the self-absorption parameter. Peimbert and Torres-Peimbert (1971*b*) and Brocklehurst (1972) from observational results and theoretical predictions found that the collisional excitation process from level 2^3S does not contribute appreciably to the intensities of λλ5876 and 4472 in planetary nebulae. On the other hand, the $2^3S - n^3D$ series with $n > 2$ is weakened by self-absorption and λλ7065, 5876 and 4472 are strengthened by resonance flourescence (Robbins 1968). The effect in the case of λ7065 is considerable while for λλ5876 and 4472 is small, but non-negligible. We have computed γ_{sa} for λλ5876 and 4472 by comparing $\{I(7065)/I(4472)\}_{obs}/\{I(7065)/I(4472)\}_{rad}$ with the computations by Robbins, normalized to the maximum values for total self-absorption presented by Cox and Daltabuit (1971). These values are based on more recent transition probabilities than those used by Robbins. From the computations of Robbins and Bernat (1973) the effect of self-absorption on λ6678 is expected to be very small and it was not considered.

From equations (20), (21), $t^2 = 0.035$, T_0(high), and the computations by Brocklehurst (1971, 1972), the y^+ and y^{++} values from the λλ4472, 5876, 6678 and 4686 lines were computed. The y^+ value was derived by giving twice as much weight to the measurement of I(5876) than to those of the other two lines. To minimize the effects of reddening and observational errors we compared λλ4472 and 4686 to Hβ and the other two lines to Hα. The y^+ and

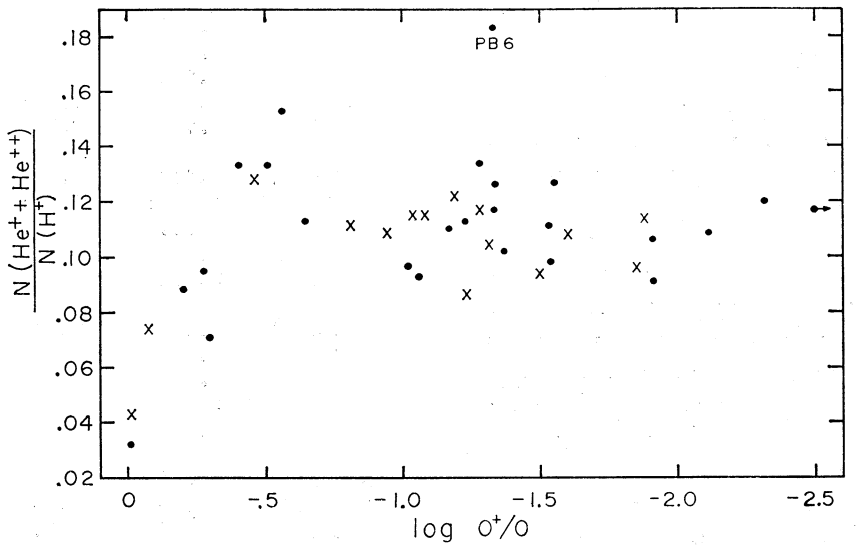

FIG. 5. Helium once and twice ionized are compared to the degree of oxygen ionization. For objects of log $O^+/O < -0.4$ there appears to be no substantial contribution due to neutral helium. Crosses are best observed objects.

y^{++} values are also presented in Table 5. The average $y^{+}(4472)$ and $y^{+}(5876)$ values for the best observed objects are 0.0876 and 0.0853, respectively. This indicates that the effect of collisional excitation from level 2^3S is negligible and that, if anything, the self-absorption effect for λ5876 has been slightly overestimated.

To obtain the total helium to hydrogen abundance ratio we have to estimate the amount of neutral helium present in each object. In Figure 5 we present $y^{+} + y^{++}$ *vs.* degree of ionization. From this figure, it is clear that for the low degree of ionization objects, defined as log $O/O^{+} < 0.4$, the $y^{+} + y^{++}$ value is systematically smaller than for the other objects, indicating that a considerable amount of helium is neutral. To estimate the fraction of neutral helium it is necessary to make observations at different distances from the ionizing star. In this paper we did not compute the total helium abundances for the PN of low degree of ionization. Alternatively, for the PN of higher degree of ionization there is no systematic trend, indicating that the amount of neutral helium is small. In what follows, this contribution to the total helium abundance has been neglected.

A considerable fraction of the scatter present in Figure 5 is due to real differences in the helium abundance. This result is discussed in §V. The helium to hydrogen abundance ratio is presented in Table 6.

b) *Carbon*

Seaton (1968*a*) has shown that, in general, the permitted lines of heavy elements are formed not only by recombination but that the excitation could also be produced by resonance fluorescence due to starlight. Kaler (1972) from observations of the I(3918.98 + 3920.68)/I(4267.02 + 4267.27) C II line intensity ratios (transitions $4s^2S - 3p^2P^0$ and $4f^2F^0 - 3d^2D$; hereinafter λλ3920 and 4267) has proposed that λ3920 is produced mainly by resonance fluorescence and λ4267 mainly by recombination. Grandi (1976) has also proposed that in the Orion Nebula a similar situation prevails.

Pengelly (1963) has computed the effective radiative recombination coefficient for λ4267. By combining Pengelly's results for case B with those for hydrogen by Brocklehurst (1971) we find

TABLE 6

TOTAL ABUNDANCES

Object	N(He)/N(H)	log N	log O	log Ne
IC 351	.098	...	8.79	8.13
IC 2003	.097	8.03:	9.02	8.32
NGC 1535	.091	...	8.58	7.97
IC 418	>.076	8.00	8.88	7.60
NGC 2022	.120	<8.76	8.81	8.05
IC 2149	>.071	7.64	8.68	7.88
IC 2165	.133	7.97	8.73	7.99
NGC 2371-2a	.134	8.74	8.81	8.19
M1-14	>.088	7.61	8.51	7.52
NGC 2392	.093:	8.24:	8.51:	7.88:
NGC 2438	>.095	8.43:	9.17:	8.59:
NGC 2440	.153	9.09	8.82	8.14
NGC 2452	.110	8.68:	8.99:	8.30:
NGC 2610b	>.109	...	8.18:	7.22:
IC 2448	.111	7.51	8.61	7.92
NGC 2792	.107	7.90:	8.78:	7.98:
PB-4	.126:	7.76:	8.63:	8.12:
NGC 2818	>.069	>8.37	>8.33	>7.91
IC 2501	.108	8.26	8.90	8.29
NGC 3132c	.128	8.68	8.98	8.56
PB-6	.183:	8.94:	8.72:	8.08:
NGC 3211	.117	8.17	8.93	8.14
NGC 3242	.108	7.71	8.72	8.03
NGC 3587	.113:	8.00:	8.65:	8.07:
NGC 3918	.112	8.28	8.90	8.16
NGC 4361	.117:	...	...	...
NGC 5307	.102	7.74	8.64	8.00
NGC 5315	.122	8.83	8.85	8.27
He2-108	>.117:	7.85:	8.40:	7.30:
IC 4406	.133:	8.52:	8.98:	8.51:
NGC 5882	.113	8.10:	8.92:	8.34:
HD 138403	>.032:	8.35:	8.65:	<8.40:
HD 141969	...	8.26:	8.38:	...
NGC 6572	.105	8.49	8.95	8.32
IC 418	>.072	8.02	8.81	7.48
NGC 6803	.115	8.72	9.02	...
NGC 7009	.114	8.44	8.93	8.37
NGC 7027	.115	8.57	9.04	...
BD+30°3639	>.043:	8.54	8.98	...
NGC 6884	.117	8.50	9.06	...
NGC 7662	.094	7.63	8.65	...
IC 5217	.086	8.04	8.73	...
NGC 1535	.096	<7.61	8.62	...
NGC 6720	.107:	>7.39	8.74	...

$$\frac{N(C^{++})}{N(H^+)} = 0.109 \left(\frac{T_{C/H\beta}}{10^4}\right)^{0.14} \frac{I(4267)}{I(H\beta)}, \quad (22)$$

where

$$T_{C/H\beta} = T_0(\text{high}) \ (1 - 1.40\ t^2) . \quad (23)$$

In equation (22) the contribution to I(4267) due to dielectronic recombination has not been taken into account. The relative contribution can be approximated by the ratio of recombination coefficients given by

$$\frac{\alpha_D}{\alpha_R} = 3 \times 10^3 \left(\frac{T_e}{10^4}\right)^{-0.9} \exp(-1.5 \times 10^5/T_e) , \quad (24)$$

(Goldberg 1968; Aldrovandi and Pequignot 1973, where there is a misprint of a factor of 10 in their listed T_0 value). From equation (24) it follows that $\alpha_D/\alpha_R < 0.1$ for $T_e < 15000°K$ and consequently for the cases considered here the dielectronic recombination can be neglected.

In Table 7 we present the $N(C^{++})/N(H^+)$ ratios derived from our observations and those derived from photographic data by Aller's group (Kaler 1976).

From the ionization structure models by Flower (1969*a*) and Rodríguez (1973) the following approximate expression was adopted

$$N(C^{+3}) = N(C^{+2}) \left[\frac{3N(O^{++})}{10N(O^+) + N(O^{++})}\right]. \quad (25)$$

It is also possible to determine $N(C^{+3})$ by means of the C III $3s^3S - 3p^3P^0$ line intensities, λλ4647.40, 4650.16 and 4651.35 (hereinafter λ4650). These lines are formed by recombination since the ground state of C III is $2s^2\ ^1S$ and the resonance fluorescence effect from a singlet state to a triplet state is negligible. The λ4650 lines are very weak and in low resolution spectra appear blended with the O II lines λλ4649.14 and 4650.84, coresponding to the transition $3s^4P - 3p^4D^0$. In general, the oxygen lines are weaker than the carbon lines, and their presence can be corroborated by the presence of other members of the multiplet. Bednarek and Clarke (see Aller *et al.* 1973) have calculated the approximate equation

TABLE 7

CARBON ABUNDANCES

Object	log C^{++}	log C^{+3} (Eq. 25)	log C^{+3} (Eq. 27)	log C (Eq. 31)
IC 351	9.0	9.3	...	9.7
IC 2003	9.1	9.1	...	9.7
NGC 1535	9.1	9.5	...	9.7
IC 418	8.9	7.7	...	8.9
NGC 2022	9.1	9.4	...	10.5
IC 2165	8.8	8.3	...	9.1
NGC 2371–2	9.0	8.9	...	9.9
NGC 2440	8.7	8.3	9.3	9.0
NGC 3242	9.0	9.3	...	9.6
NGC 3918	<9.3	<9.1	...	<9.7
NGC 6572	8.8	9.1	...	9.3
NGC 6803	8.7	8.9	...	9.1
NGC 7009	9.1	9.5	9.5	9.7
NGC 7027	8.9	8.9	9.3	9.4
BD + 30°3639	7.7	5.2	...	...
NGC 6884	9.1	9.3	...	9.6
NGC 7662	9.1	9.4	9.6	9.8
IC 5217	8.8	9.0	...	9.2
NGC 6720	9.0	9.4	...	>9.8

$$\frac{N(C^{+3})}{N(H^+)} = 0.46 \left(\frac{T_e}{10000}\right)^{-0.28} \frac{I(\lambda 4650)}{I(H\beta)}. \quad (26)$$

This equation does not include dielectronic recombination which for $C^{+3} \rightarrow C^{+2}$ is very important. Equation (26) can be modified to include dielectronic recombination as follows

$$\frac{N(C^{+3})}{N(H^+)} = 0.46 \left(\frac{T_e}{10000}\right)^{-0.28} \times \frac{1}{(1 + \alpha_D/\alpha_R)} \frac{I(4650)}{I(H\beta)}, \quad (27)$$

where

$$\alpha_D/\alpha_R = 1.2 \times 10^3 \left(\frac{T_e}{10^4}\right)^{-0.73} \exp(-91000/T_e) \quad (28)$$

(Aldrovandi and Pequignot 1973).

In Table 7 we present the $N(C^{+3})$ values derived from equations (25) and (27); where the I(4650) values were taken from photometric line intensities in the literature (Kaler 1976). For NGC 7662 and NGC 7009 the agreement between both relations is very good. However for NGC 2440 and NGC 7027 equation (27) yields considerably higher $N(C^{+3})$ values. Equation (22) is more reliable than equation

(27) and in general the measurements of I(4267) are of higher accuracy than those of I(4650). Consequently in what follows the $N(C^{+3})$ values derived from equation (27) were not considered.

To obtain the total carbon abundance it is necessary to correct for the unobserved stages of ionization. For IC 418 the model of Flower (1969*b*) yields

$$\frac{N(C)}{N(H)} = i_{cf}(C)\,\frac{N(C^{+2})}{N(H^{+})} = 1.47\,\frac{N(C^{+2})}{N(H^{+})}, \qquad (29)$$

where most of the unobserved carbon is in the form of C^{+}.

C^{+} is important only in objects with a substantial amount of neutral helium like IC 418; and in general for the PN of higher degree of ionization carbon is expected to be only in the form of C^{+2} to C^{+4}. From the ionization potentials of carbon and helium and from the theoretical models by Flower (1969*a*) and Rodríguez (1973) we have adopted the following expression

$$N(C^{+4}) = \frac{y^{++}}{y^{+}}[N(C^{+2}) + N(C^{+3})], \qquad (30)$$

which can be coupled to equation (25) to yield:

$$\frac{N(C)}{N(H)} = \left(1 + \frac{y^{++}}{y^{+}}\right)\left(1 + \frac{3N(O^{++})}{10\,N(O^{+}) + N(O^{++})}\right) \times \frac{N(C^{++})}{N(H^{+})} = i_{cf}(C)\,\frac{N(C^{++})}{N(H^{+})}. \qquad (31)$$

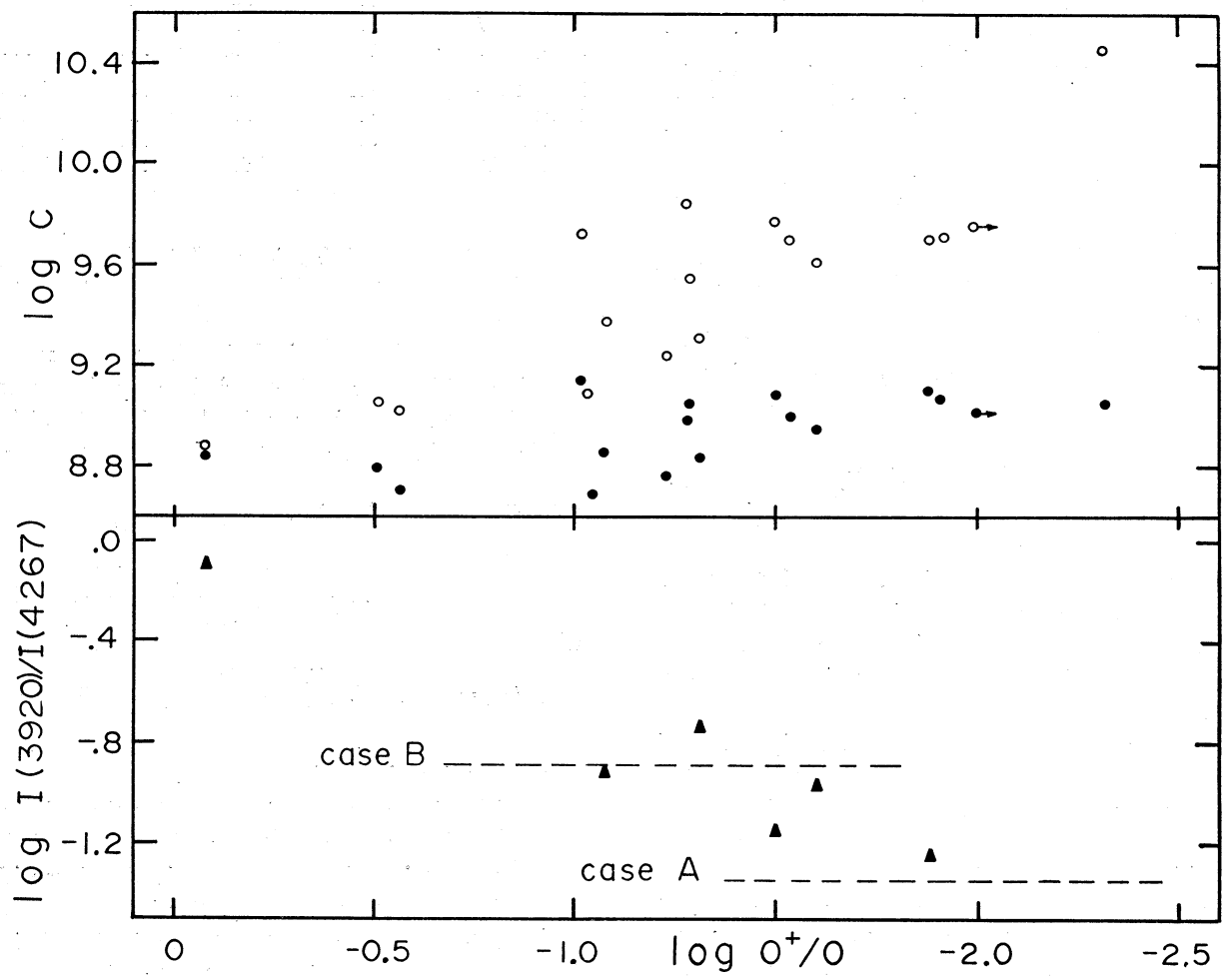

FIG. 6. Carbon abundance compared to the degree of oxygen ionization. *a*) Filled circles are log C^{+2} and circles are log C. *b*) Ratio of line intensities of C^{+2}. The broken lines correspond to radiative recombination ratios according to Pengelly (1963).

In Table 7 we present the total carbon abundance. The $i_{cf}(C)$ given by equation (31) becomes very large and rather uncertain for NGC 2022 and NGC 2371. In any case $i_{cf}(C) > (1 + y^{++}/y^{+})$ and log N(C) is higher than 9.4 and 9.5 for NGC 2022 and NGC 2371, respectively. In Figure 6 we present the $N(C^{+2})/N(H)$ and the N(C)/N(H) abundance ratios *vs.* the degree of ionization.

These results are unexpected not only because the $N(C^{+2})/N(H^{+})$ ratio is already substantially higher than the N(C)/N(H) value derived for the Orion Nebula (see §IV*e*), but also because the N(C)/N(H) ratio increases with the degree of ionization. We have analyzed these results further. The values in Table 7 and Figure 6*a* were derived under the assumption that the λ4267 line is formed only by recombination, and consequently that it is proportional to $N(C^{+2})$. On the other hand, it is possible that some contribution to the intensity of this line is produced by resonance fluorescence, which is proportional to $N(C^{+})$. From ionization structure models (Flower 1969*b*; Rodríguez 1973; Peimbert *et al.* 1974) it is expected that $N(C^{+})/N(C) < N(O^{+})/N(O)$. Therefore, the higher the degree of ionization, the smaller the $N(C^{+})/N(C)$ ratio, and consequently the smaller the contribution due to the resonance fluorescence effect to λ4267.

Moreover, in Figure 6*b* we have plotted the observed ratio I(3920)/I(4267) *vs.* O^{+}/O. These ratios are from photographic measurements of very weak lines (Kaler 1976), therefore errors as large as a factor of two are to be expected. The dotted lines represent the theoretical ratios predicted under cases A and B for radiative recombination (Pengelly 1963). It is possible that for very extended objects with a small amount of C^{+}, the λλ3920 and 4267 lines originate in a situation closer to case A than to case B. From the computations of Pengelly the effect of assuming case A instead of case B is that the predicted emissivity of λ4267 decreases by less than 1% while that of λ3920 decreases by a factor of 3. The abundances derived from I(4267) are practically independent of the case assumed.

From Figure 6*b* and a similar one by Kaler (1972), where he plots I(3920)/I(4267) *vs.* T_{star}, is follows that for the PN of high degree of ionization not only λ4267 is formed by recombination but also λ3920. Alternatively, for objects of lower degree of ionization, (left hand region of Figure 6) a substantial fraction of I(3920) is due to resonance fluorescence, RF. Since λ3920 is a s-p transition and λ4267 a f-d transition, a considerably smaller contribution due to RF is expected for I(4267) (Kaler 1972; Grandi 1976). In any case, if a small contribution to I(4267) due to RF was present, it would produce an even higher increase in the carbon abundance with ionization degree.

There are two possible explanations for this effect: *a*) that in the early stages of evolution of a PN, when it is still optically thick, a substantial amount of carbon in the envelope is in the form of dust grains (Panagia *et al.* 1976). These grains might be destroyed at later stages of evolution. And/or *b*) that the stellar mass ejected during the expansion of the shell (Mathews 1966) is very rich in carbon while the initially ejected shell is not as rich.

There is additional evidence in favor of the carbon rich nature of PN from the observation of the C IV λ1549 and C III] λ1909 lines in NGC 7027 (Bohlin *et al.* 1975; Panagia *et al.* 1976) and in NGC 7662 (Stecher 1976). For these objects it is found that log C ~ 8.8 − 9.0 in gaseous form; and Panagia *et al.* estimate that a similar fraction of carbon atoms is embedded in dust grains in NGC 7027, which raises the total carbon abundance to log C ~ 9.1 − 9.3. These ultraviolet lines are very sensitive to the electron temperature adopted. From the temperatures presented in Table 4 even higher carbon abundances are derived from the λλ1549 and 1909 line intensities.

The spectra of the central stars of PN also seem to indicate a carbon overabundance. According to Smith and Aller (1969) for 27 PN nuclei with emission lines: five are WC, one is WN, and five are of the WR-Of type showing carbon lines in emission. The spectroscopic appearance of the WR nuclei of PN is very similar to that of population I WR stars. The difference between both types of objects is the absolute magnitude of the central star and the mass of the nebular envelope. The usual interpretation for the spectral appearance of population I WR stars of the carbon sequence is that they are carbon rich (Paczynski 1973; Smith 1973). For example, an overabundance of an order of magnitude has been estimated for the WC8 component of γ^{2} Velorum (Castor and Nussbaumer 1971). Moreover,

of the six Of central stars, five show very strong carbon lines in emission, in contradistinction to population I Of stars.

It is found that in the PN of the solar neighborhood nitrogen is overabundant with respect to H II regions (see §IV*e*); which implies that part of the nebular matter in PN has been processed through the CNO cycle. In this case, carbon is almost completely transformed into nitrogen before any appreciable amount of helium is transformed into hydrogen (cf. Torres-Peimbert and Peimbert 1971). If the ejected material had been contaminated only by this process, carbon would be underabundant instead of overabundant. The carbon overabundance implies that there has been additional enrichment by material that has undergone helium burning.

The overabundance of carbon should be verified due to the importance that this result has for the study of the nature of PN and in general of galactic evolution. It is particularly important to observe the λλ1549 and 1909 lines in objects of different degree of ionization, low reddening and well established electron temperature. An attempt ssould be made to determine accurate C^{+3} and C^{+4} abundances from the C III and C IV lines that arise mainly by recombination (Grandi 1976). For this, accurate radiative and dielectronic effective recombination coefficients are needed, as well as more accurate line intensity measurements in objects of various degrees of ionization.

d) *Effect of t^2 on the abundance determinations*

In Table 8 we present the total abundances for NGC 3918 and NGC 6572 for three values of t^2,

TABLE 8

ABUNDANCES AND SPATIAL TEMPERATURE FLUCTUATIONS

	NGC 3918			NGC 6572		
Element	$t^2 = 0$	0.035	0.055	0	0.035	0.055
He/H	0.113	0.112	0.112	0.107	0.105	0.105
log C	<9.7	<9.7	<9.7	9.3	9.3	9.3
log N	8.16	8.27	8.41	8.28	8.49	8.63
log O	8.76	8.89	8.99	8.73	8.95	9.11
log Ne	8.01	8.15	8.21	8.09	8.32	8.49

the mean square temperature fluctuation. The value of $t^2 = 0$ corresponds to the case of two different zones of uniform temperatures T_0(low) = T(N II) and T_0(high) = T(O III). This case yields the highest average temperatures and provides us with an absolute lower limit to the heavy element abundance derived from forbidden lines. The values for $t^2 = 0.055$ is probably an extreme case in the opposite direction. From Table 8 it follows that to obtain accurate abundances from emission lines produced by collisional excitation relative to lines produced by recombination, it is necessary to derive the t^2 value corresponding to the observed volume. Alternatively, the relative abundances in the visual region derived only from collisionally excited lines or only from recombination lines are almost independent of t^2. That is, He/H, C/H, Ne/O and N/O are not sensitive to the adopted t^2.

e) *Comparison with other abundance determinations*

We have taken the average chemical composition of the best observed PN and it is presented in Table 9 as representative for PN of the solar neighborhood. Also in Table 9 we present the chemical composition of PN derived by other authors (Aller and Czyzak 1968, 1973; Baker 1974; Peimbert and Torres-Peimbert 1971*b*). In the case of Baker we listed his results for population I objects. In the case of Peimbert and Torres-Peimbert the helium abundance listed neglects the collisional excitation from the helium 2^3S level. From Tables 6 and 7 it can be seen that the chemical composition of PN varies from object to object. This variation is real, and is probably related to the initial chemical composition of the parent star and consequently to the position in the galaxy at the time of formation (see §V).

Taking this into account, and the fact that the atomic parameters used to derive abundances are slightly different, the agreement among the various determinations is good.

Also in Table 9 we present the abundances derived for the Orion Nebula (Peimbert and Torres-Peimbert 1977) using exactly the same observational procedure and atomic parameters as those used here. In the last column of Table 9 we include the solar photospheric abundance of C, N and O de-

TABLE 9

COMPARISON OF CHEMICAL COMPOSITION

Object	He	C	N	O	Ne	Reference*
PN	11.04	9.5	8.33	8.87	8.28	This paper
PN	11.04	...	8.24	8.76	...	PTP71
PN	11.06	...	7.79	8.51	7.83	B74
PN	11.09	<8.7	8.12	8.85	8.2	AC73
PN	11.23	...	8.1	8.9	7.9	AC68
Orion	11.00	8.52	7.76	8.75	7.90	PTP77
Sun	...	8.55	7.93	8.77	7.97	L68,B72

*Aller and Czyzak 1968, 1973; Baker 1974; Bertsch *et al.* 1972; Lambert 1968; Peimbert and Torres-Peimbert 1971*b*, 1977.

ived by Lambert (1968) together with the neon abundance derived from the Ne/O solar flare cosmic rays ratio (Bertsch et al. 1972) normalized to the oxygen photospheric abundance.

In addition, and independently of the apparent overabundances of carbon reported in §IV*c*, we have three observational restrictions to impose to the conditions of formation of PN shells: 1) Nitrogen is overabundant; this effect is not connected with the degree of ionization of nitrogen (Figure 3) and thus it is unlikely to be due to errors in the reduction. It appears to be connected with the general evolution of the galaxy (§V); 2) The N(He)/N(H) ratios for PN of the solar neighborhood and that of the Orion Nebula are very similar (Table 9). Moreover we do not find any systematic effects in the N(He)/N(H) ratio in Figure 5 between objects of moderate and high degree of ionization. Only a very small amount of helium-rich material could have been ejected to the interstellar medium, since the PN as a group, appear to have only ~10% more helium than Orion. Of the 36 objects of intermediate and high ionization for which He/H was derived, only PB6 shows significantly more helium; unfortunately, the line intensities for this object are not very accurate, and this result should be confirmed. 3) The N(O)/N(H) values for PN, the Orion Nebula, and the Sun are very similar (Table 9); therefore oxygen production after the 3α reaction has not been substantial in the ejected material. From Figure 7 it can be seen that the derived oxygen abundance is not correlated to the ionization degree; which implies that any solar wind present after the ejection of the main shell is not substantially overabundant in oxygen.

V. ABUNDANCE GRADIENTS AND CHEMICAL EVOLUTION

In figure 8 we show the helium, oxygen, and nitrogen abundances *vs.* R, the galactocentric distance presented in Table 4. There is a general trend in the sense that the smaller the value of R the larger the abundances of these elements relative to hydrogen. Also in Figure 8 we show the least squares fit to the best observed PN. In Table 10 we present the numeric values for the corresponding helium, oxygen and nitrogen abundance gradients for the

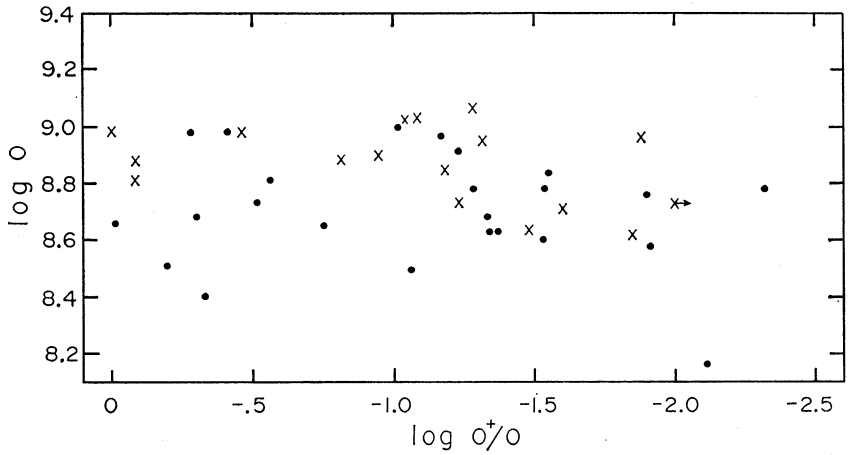

FIG. 7. Oxygen abundance compared to the degree of oxygen ionization. No systematic effects are found. Crosses are best observed objects.

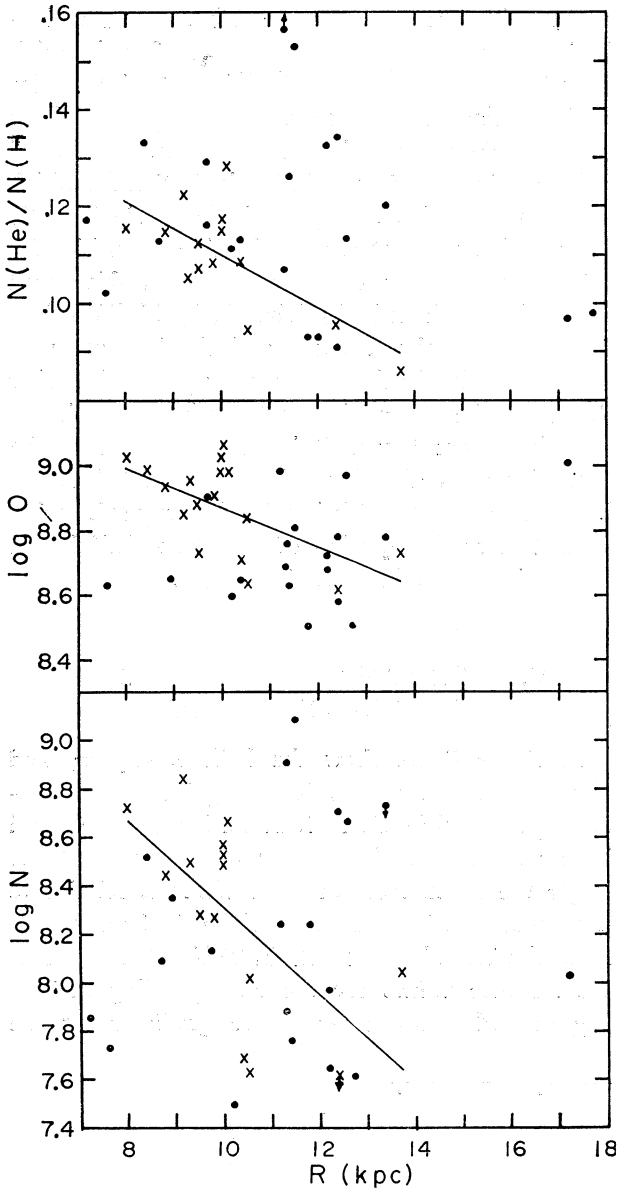

FIG. 8. Abundance of helium, oxygen and nitrogen compared to the galactocentric distance. A value of $R_{\odot} = 10$ kpc was adopted. Although individual distances may be in error, in general the objects closer to the galactic center are richer in He, O and N than those in the anticenter direction. Crosses are best observed objects. Lines are least squares solutions to best observed objects.

best observed PN. Also presented here are the metallicity gradients derived by Mayor (1976) from an analysis of the kinematic and photometric properties of about 600 dF stars and 600 gG-gK stars. The steepest one corresponds to a subset of the sam-

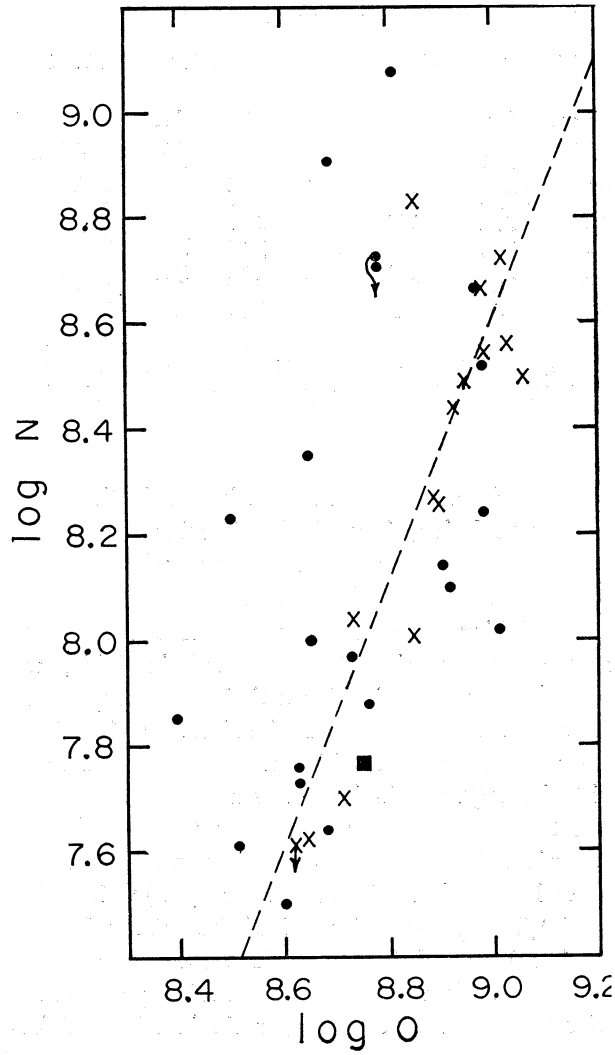

FIG. 9. Comparison of nitrogen and oxygen abundances Crosses are best observed objects. Broken line is the leas squares solution of slope 2.5.

TABLE 10

SOLAR NEIGHBORHOOD ABUNDANCE GRADIENTS

X	$\frac{d \log(X/H)}{dR}$ (kpc^{-1})
He	$-0.02 \pm .01$
O	$-0.06 \pm .02$
N	$-0.18 \pm .04$
M (all stars)*	$-0.05 \pm .01$
M (young stars)*	$-0.10 \pm .02$

* Metallicity from dF, gG and gK stars (Mayor 1976)

ple comprising the youngest objects. The value for the oxygen gradient derived from PN (representing the Z gradient), agrees very well with the value for the metallicity gradient of the complete stellar sample.

Even if very tightly correlated abundance gradients across the disk of our galaxy had been present when the parental stars of the PN were formed there are at least three effects that would have masked these gradients: 1) The observational errors in the line intensity ratios tend to destroy the correlation. 2) The assigned distances to individual PN may be incorrect; they are based on statistical distance scales. 3) Since PN are not extreme population I objects their present galactocentric distance may be substantially different than the distance at the time of formation of the parent stars.

Due to the uncertainties listed above, we believe it is more dependable to study the presence of abundance correlations independent of individual distances, like those in Figures 9 to 11. In these figures, again the correlations are tighter for the best observed PN than for the other objects. This implies that the correlations are real. A substantial fraction of the scatter is due to observational errors and not to the method used to derive the chemical abundances, since errors in the determination of the temperature tend to destroy the correlations.

In Figure 9 we present N(N)/N(H) *vs.* the N(O)/N(H) abundance ratios. We have adjusted a least squares fit to the best observed PN which yields $\Delta[N/H]/\Delta[O/H] = 2.5$, where the square brackets refer to the usual logarithmic notation. Smith (1975) from observations of H II regions in spiral galaxies found that $\Delta[N/H]/\Delta[O/H] \sim 1.5$. Furthermore by comparing the SMC H II regions with the Orion Nebula (Peimbert and Torres-Peimbert 1977) a value of 1.4 is derived, in very good agreement with the determination by Smith. In any case, it is clear that the N/O ratio derived from PN is considerably larger than that derived from H II regions. From Table 5 and Figure 9 nitrogen appears to be appreciably modified by the evolution of the parental star, while oxygen does not. Boeshaar (1975) had already found that in general for PN, the earlier the population type of the object, the more abundant in nitrogen.

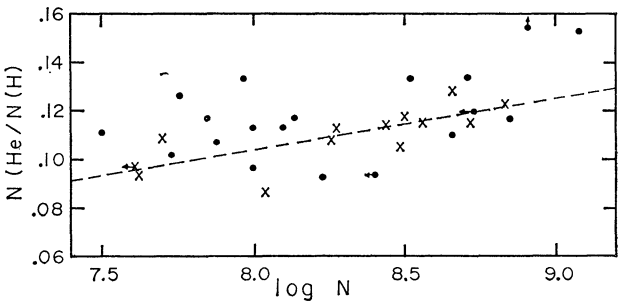

FIG. 10. Comparison of helium and nitrogen abundances. Crosses are best observed objects. Broken line is the least squares solution.

In Figure 10 we show a plot of the N(He)/N(H) *vs.* the N(N)/N(H) abundance ratio; these elements appear to be correlated. Baker (1974) had previously found a similar correlation.

The N(Ne)/N(O) and N(O)/N(H) abundance ratios are very similar in H II regions and PN (see Table 9) and since oxygen is the most abundant heavy element in the solar neighborhood we will use it as a tracer of the heavy element abundance content, Z. Therefore following Peimbert and Torres-Peimbert (1974) we will assume Z to be directly proportional to O/H, and for $\log N(O)/N(H) = -3.42$ we will adopt $Z = 0.01$.

In Figure 11 we present the Y *vs.* Z diagram where we have included the values for the SMC H II regions (Peimbert and Torres-Peimbert 1976) and for the Orion Nebula (Peimbert and Torres-Peimbert 1977). It is clear again, that Y and Z are correlated in PN and that the slope is similar to that derived from H II regions. A least squares fit to the best observed PN yields a ratio of the rate of helium enrichment to the rate of heavy element enrichment, $\Delta Y/\Delta Z = 2.4$. This result is in good agreement with the value derived from H II regions, which is 3.3 ± 0.6 (Peimbert and Torres-Peimbert 1977). The similarity between both ratios probably indicates that the helium and oxygen abundances of the envelope have not been substantially affected by the products of the evolution of the PN parental star, and that $\Delta Y/\Delta Z$ in the envelopes of PN corresponds to that of the material that formed the parental star.

The $\Delta Y/\Delta Z$ values for H II regions and PN are considerably higher than the theoretical values which

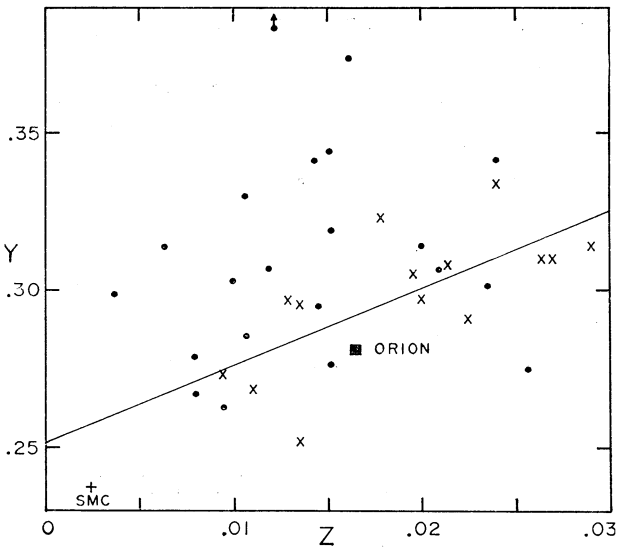

FIG. 11. Comparison of helium and heavy element abundances. It has been assumed that Z ∝ O. Crosses are best observed objects. Line is the least squares solution of slope 2.4. Orion and the H II regions in the SMC have also been indicated for comparison.

range from 0.3 to 1 (Hacyan *et al.* 1976; Gingold 1977). The theoretical values are derived by assuming: 1) A model of chemical evolution for the galaxy. 2) An initial mass function. 3) A set of values for the composition of the ejected material, for stars of various masses, derived from stellar evolution studies. It seems that the discrepancy between the predicted and observed values of $\Delta Y/\Delta Z$ can be solved by considering helium rich mass loss from massive stars in their pre-supernova stage. This has not been considered in the stellar evolution predictions of the ejected material. From *Copernicus* observations there is observational evidence for substantial mass loss in very massive stars, practically in all the observed stars earlier than B1 (Snow and Morton 1976; Conti and Frost 1977). Furthermore, in the case of WR stars of population I the present mass loss is helium rich (Smith 1973).

It is possible to improve the study of the composition gradient in the galaxy from planetary nebulae and the ratio of the rates of enrichment, $\Delta Y/\Delta Z$ in their envelopes. For this, a set of highly accurate photoelectric line intensities are needed in more objects. In particular a better knowledge of the ionization correction factors would be very useful. This could be obtained from line intensities at different distances from the ionizing star or of filaments of high and low degree of ionization. However, considering that the correlations in Figures 9-11 were derived from objects of widely different ionization degrees, temperatures and densities we do not expect the general picture to change drastically.

We would like to acknowledge the assistance provided by the KPNO staff with the operation of the IIDS and reduction of the data, in particular we woud like to mention J. B. DeVeny and B. Johnson. We are grateful for the hospitality of the staff of the Dept. of Physics and Astronomy, University College, London, where part of this paper was prepared. Helpful comments were received from M. J. Seaton. We thank I. Cruz-González and J. F. Rayo for their help in various aspects of this investigation.

REFERENCES

Aldrovandi, S. M. V., and Pequignot, D. 1973, *Astron. & Astrophys.*, **25**, 137.
Aller, L. H., and Czyzak, S. J. 1968, *Planetary Nebulae*, ed. D. E. Osterbrock and C. R. O'Dell (Dordrecht: Reidel), p. 209.
Aller, L. H., and Czyzak, S. J. 1973, *Mém. Soc. Roy. Sci. Liège*, 6e. ser, **5**, 285.
Aller, L. H., and Faulkner, D. J. 1964, in *The Galaxy and the Magellanic Clouds*, I. A. U. Symposium No. 20, p. 45.
Baker, T. 1974, Ph. D. thesis, Univ. California, Santa Cruz.
Balick, B., and Sneden, C. 1976, *Ap. J.*, **208**, 336.
Bertsch, D. L., Fichtel, C. E., and Reames, D. V., 1972, Ap. J., **171**, 169.
Boeshaar, G. 1975, *Ap. J.*, **195**, 695.
Bohlin, R. C., Marionni, P. A., and Stecher, T. P. 1975, *Ap. J.*, **202**, 415.
Brocklehurst, M. 1971, *M.N.R.A.S.*, **153**, 471.
Brocklehurst, M. 1972, *M.N.R.A.S.*, **157**, 211.
Cahn, J. H., and Kaler, J. B. 1971, *Ap. J. Suppl.*, **22**, 319.
Castor, J. I., and Nussbaumer, H. 1971, *Bull. Am. Astron. Soc.*, **3**, 378.
Code, A. D. 1960, in *Stellar Atmospheres*, ed. J. L. Greenstein (Chicago: University of Chicago Press), p. 50.
Conneely, M. J., Smith, K., and Lipsky, L. 1970, *J. Phys. B.: Atom. Molec. Phys.*, **3**, 493.
Conti, P. S., and Frost, S. A. 1977, *Ap. J.*, **212**, 728.
Cox, D. P., and Daltabuit, E. 1971, *Ap. J.*, **167**, 257.
Cudworth, K. M. 1974, *A. J.*, **79**, 1384.
Czyzak, S. J., and Krueger, T. K. 1963, *M.N.R.A.S.*, **126**, 177.
Czyzak, S. J., Krueger, T. K., Martins, P. de A. P., Saraph, H. E., Seaton, M. J., and Shemming, J. 1968, in *Planetary Nebulae*, ed. D. E. Osterbrock and C. R. O'Dell (Dordrecht: D. Reidel), p. 138.

'Odorico, S., Peimbert, M., and Sabbadin, F. 1976, *Astron. & Astrophys.*, **47**, 341.
issner, W., and Seaton, M. J. 1974, *J. Phys*, B.: *Atom. Molec. Phys.*, **7**, 2533.
lower, D. R. 1969*a*, *M.N.R.A.S.*, **146**, 171.
lower, D. R. 1969*b*, *M.N.R.A.S.*, **146**, 243.
arstang, R. H. 1968, in *Planetary Nebulae*, ed. D. E. Osterbrock and C. R. O'Dell (Dordrecht: D. Reidel), p. 143.
ingold, R. A. 1977, *M.N.R.A.S.*, **178**, 569.
oad, L. E., Goldberg, L., and Greenstein, J. L. 1972, *Ap. J.*, **175**, 117.
oldberg, L. 1968, in *Interstellar Ionized Hydrogen*, ed. Y. Terzian (Benjamin: New York), p. 373.
randi, S. A. 1976, *Ap. J.*, **206**, 658.
acyan, S., Dultzin-Hacyan, D., Torres-Peimbert, S., and Peimbert, M. 1976. *Rev. Mex. Astron. Astrof.*, **1**, 355.
awley, S. A., and Miller, J. S. 1977, *Ap. J.*, **212**, 94.
ayes, D. S. 1970, *Ap. J.*, **159**, 165.
ayes, D. S., and Latham, D. W. 1975, *Ap. J.*, **197**, 593.
aler, J. B. 1972, *Ap J.*, **173**, 601.
aler, J. B. 1976, *Ap. J. Suppl.*, **31**, 517.
aler, J. B., Aller, L. H., Czyzak, S. J., and Epps, H. W. 1976, *Ap. J. Suppl.* **31**, 163.
ambert, D. L. 1968, *M.N.R.A.S.*, **138**, 143.
athews, W. G. 1966, *Ap. J.*, **143**, 173.
ayor, M. 1976, *Astron. & Astrophys.*, **48**, 301.
inkowski, R. 1965, in *Galactic Structure*, ed. A. Blaauw and M. Schmidt (Chicago: University of Chicago Press), p. 321.
ussbaumer, H. 1971, *Ap. J.*, **166**, 411.
'Dell, C. R. 1962, *Ap. J.*, **135**, 371.
'Dell, C. R. 1963*a*, *Ap. J.*, **138**, 67.
'Dell, C. R. 1963*b*, *Ap. J.*, **138**, 293.
'Dell, C. R. 1968, in *Planetary Nebulae*, ed. D. E. Osterbrock and C. R. O'Dell (Dordrecht: D. Reidel), p. 361.
ke, J. B. and Schild, R. E. 1970, *Ap. J.*, **161**, 1015.
sterbrock, D. E. 1973, *Mém. Soc. Roy. Sci. Liège*, 6e. ser, **5**, 391.
aczynski, B. 1973, in *Wolf-Rayet and High-Temperature Stars*, ed. M. K. V. Bappu and J. Sahade (Dordrecht: D. Reidel), p. 143.
anagia, N., Bussoletti, E., and Blanco, A. 1976, preprint.
eimbert, M. 1967, *Ap. J.*, **150**, 825.
eimbert, M. 1971, *Bol. Obs. Tonantzintla y Tacubaya*, **6**, 29.
Peimbert, M., and Costero, R. 1969, *Bol. Obs. Tonantzintla y Tacubaya*, **5**, 3.
Peimbert, M., and Torres-Peimbert, S. 1971*a*, *Bol. Obs. Tonantzintla y Tacubaya*, **6**, 21.
Peimbert, M., and Torres-Peimbert, S. 1971*b*, *Ap. J.*, **168**, 413.
Peimbert, M., and Torres-Peimbert, S. 1974, *Ap. J.*, **193**, 327.
Peimbert, M., and Torres-Peimbert, S. 1976, *Ap. J.*, **203**, 581.
Peimbert, M., and Torres-Peimbert, S. 1977, *M.N.R.A.S.*, **169**, 217.
Pengelly, R. M. 1963, *Ph. D. thesis*, University of London.
Perek, L., and Kohoutek, L. 1967, *Catalog of Galactic Planetary Nebulae*, (Prague: Czechoslovakian Acad. of Sci.).
Pradhan, A. K. 1974, *J. Phys. B.: Atom. Molec. Phys.*, **7** L503.
Pradhan, A. K. 1976*a*, *M.N.R.A.S.*, **177**, 31.
Pradhan, A. K. 1976*b*, private communication.
Robbins, R. R. 1968, *Ap. J.*, **151**, 511.
Robbins, R. R., and Bernat, A. P., 1973, *Mém. Soc. Roy. Sci. Liège*, 6e. ser, **5**, 263.
Rodríguez, L. F. 1973, B. S. thesis, Universidad Nacional Autónoma de México.
Saraph, H. E., and Seaton, M. J. 1970, *M.N.R.A.S.*, **148**, 367.
Seaton, M. J. 1966, *M.N.R.A.S.*, **132**, 113.
Seaton, M. J. 1968*a*, *M.N.R.A.S.*, **139**, 129.
Seaton, M. J. 1968*b*, *Astrophys. Letters*, **2**, 55.
Seaton, M. J. 1975, *M.N.R.A.S.*, **170**, 475.
Seaton, M. J., and Osterbrock, D. E., 1957, *Ap. J.*, **125**, 66.
Shklovsky, I. S. 1956, *Soviet Astr. A. J.*, **33**, 315.
Smith, H. E. 1975, *Ap. J.*, **199**, 591.
Smith, L. F. 1973, in *Wolf-Rayet and High Temperature Stars*, ed. M. K. V. Bappu and J. Sahade (Dordrecht: D. Reidel), p. 15.
Smith, L. F., and Aller, L. H. 1969 *Ap. J.*, **157**, 1245.
Snow, T. P., and Morton, D. C. 1976, *Ap. J. Suppl.*, **32**, 429.
Stecher, T. P. 1976, oral communication to IAU Commision 34, Grenoble.
Stone, R. P. S. 1974, *Ap. J.*, **193**, 135.
Torres-Peimbert, S., and Peimbert, M. 1971, *Bol. Obs. Tonantzintla y Tacubaya*, **6**, 101.
Webster, E. L. 1969, *M.N.R.A.S.*, **143**, 79.
Whitford, A. E. 1958, *A. J.*, **63**, 201.